A Study of the Depolarization of Lunar Radar Echoes

Tor Hagfors

Lincoln Laboratory,* Massachusetts Institute of Technology

ABSTRACT

39959

The radar backscattering characteristics of the lunar surface are examined in detail at a wavelength of 23 cm. The backscattered waves are studied both for circular and for linear polarization of the transmitted wave. Effects relating to the orientation of the local plane of incidence on the moon with respect to the polarization of transmitted or scattered waves are investigated. The experimental results appear to strongly support the hypothesis that the returns at oblique angles of incidence arise through single scattering from discrete objects as opposed to the returns at near normal incidence which are dominated by quasispecular reflection.

Author

GPO PRICE $ ______

CFSTI PRICE(S) $ ______

Hard copy (HC) 2.00

Microfiche (MF) .50

ff 653 July 65

FACILITY FORM 602

N66 39959 (ACCESSION NUMBER)

(THRU) 1

49 (PAGES)

(CODE) 30

CR-79098 (NASA CR OR TMX OR AD NUMBER)

(CATEGORY)

----

*Operated with support from the U. S. National Aeronautics and Space Administration under Contract No. NSR 22-009-106.

1. Introduction

The moon has been subjected to rather intensive studies by earth-based radars over the last few years. Most of these studies have been carried out in order to derive information about the physical properties of the lunar surface; some studies have also been devoted to the question of orbit parameters of the moon.

Several different experimental procedures are available for deriving information about lunar surface properties. Measurements of the total lunar cross section have been carried out in the wavelength region from 8 mm to 22 m (Evans and Pettengill, 1963a; Davis and Rohlfs, 1964). Values of the cross section can be interpreted in terms of electrical properties of the surface material based on various models of the lunar surface. The most credible interpretations of the data at the moment appear to indicate that the dielectric constant of the surface material for wavelengths of a few decimeters is about 2.6 – 2.7 (Evans and Hagfors, 1964; Rea et al, 1964). These estimates, however, are based on the assumption that the lunar surface is homogeneous with depth and that an abrupt transition from vacuum to a dielectric medium takes place at the interface.

Measurements of the delay spread of the lunar echoes have been used to derive the backscattering cross section per unit solid angle per unit surface area as a function of angle of incidence. The angular variation of this cross section in turn has been used to derive certain statistical properties of the slopes of the lunar surface (Hagfors, 1961; Daniels, 1963; Beckmann, 1964). Although there is general agreement about the interpretation of the echoes for small angles of incidence, the interpretation for larger angles is at present a subject of dispute. Some authors maintain that the returns even at large angles of incidence can be described in the usual Kirchhoff approximation if proper allowance is made for the geometric shadowing of the surface (Beckmann and Klemperer, 1965; Beckmann, 1965). Others maintain the view that the scattering at larger angles of incidence can best be thought of as returns from individual discrete scatterers of size comparable with the wavelength of observation (Evans and Pettengill, 1963b; Evans and Hagfors, 1966).

More refined observation techniques have been developed to discriminate between different areas on the moon (Pettengill and Henry, 1962). These methods have been used to study the reflectivity of many features on the lunar surface (Thompson, 1965). It has been found that many craters, particularly rayed or younger ones, exhibit enhanced reflectivity at oblique incidence.

Most radar observations of the moon are carried out with circular polarization at the transmitter and with the receiver adjusted for the orthogonal circularly polarized wave. Observations have also been made in which the same circular polarization is received as was transmitted. Since this component should contain no energy in the case of an ideal reflector, this component has been termed "depolarized" (Evans and Pettengill, 1963b). Extensive depolarization studies of this type have been carried out at 68 and 23 cm wavelength (Evans and Hagfors, 1966). The study of the depolarization of lunar echoes using circularly polarized waves, however, does not exhaust the possibilities for polarization observations. There are many other combinations of transmit and receive polarizations which may yield independent data on the scattering properties of the surface. Examples of such additional polarization studies have been published previously (Hagfors et al, 1965; Evans and Hagfors, 1966) in preliminary form. The present theoretical understanding of scattering from rough surfaces does not appear to be sufficiently well developed to be capable of fully utilizing the more complete measurements of depolarization properties discussed in this paper to make further deductions about the physical state of the lunar surface material. It will be shown, however, that a number of physically plausible conclusions can indeed be drawn from the observational results — at least in a heuristic manner.

In the following sections it is first discussed how many different measurements are required for the complete electromagnatic determination of the backscattering properties of the surface in a statistical manner. Because of the statistical nature of the problem the transmitted and received radiation is adequately described in terms of second order moments of the transverse fields — or in terms of Stokes vector. The lunar surface is characterized by quantities relating various second order moments of the radiation transmitted to those received — or in terms of a Mueller matrix. As the radar system used calls for certain capabilities not commonly found in radar systems, the equipment used is very briefly described in the third section of the paper. The fourth section contains a number of observational results obtained from the Millstone Hill radar at a wavelength of 23 cm and also some preliminary observational results from the Haystack radar at a wavelength of 3.8 cm. Section 5 discusses at some length the significance of the observational results in terms of various physical models of the lunar surface, and also in the light of observational material from experiments not involving radar observations.

2. Electromagnetic Description of the Scattering Process

A partly polarized plane electromagnetic wave traveling along the positive z-direction may be represented as:

$$\vec{E}\,(z,t) = \vec{E}_o(t)e^{\,i(\omega t-kz)} \tag{1}$$

where $\vec{E}_o(t)$ is a slowly varying time function. The vector $\vec{E}_o(t)$ may be decomposed along two orthogonal directions, both orthogonal to the direction of propagation of the wave. The components along these directions, represented by unit vectors $\vec{e}_1$ and $\vec{e}_2$, will in general be complex phasors. When the field is a Gaussian process, every statistical property of the field may be found from the second order moments of the various phasor components. If $\vec{e}_1$ and $\vec{e}_2$ correspond to the x and the y directions respectively the field is thus completely specified by:

$$\langle |E_x|^2 \rangle \,,\ \langle |E_y|^2 \rangle,\ \langle E_x E_y^* \rangle \text{ and } \langle E_y E_x^* \rangle$$

The usual Stokes vector representation involves the following four linearly independent combination of these moments.

$$\begin{aligned} S_1 &= \langle |E_x|^2 + |E_y|^2 \rangle \\ S_2 &= \langle |E_x|^2 - |E_y|^2 \rangle \\ S_3 &= \langle E_x E_y^* + E_y E_x^* \rangle \\ S_4 &= i\, \langle E_x E_y^* - E_y^* E_x^* \rangle \end{aligned} \tag{2}$$

Physically S_1 is proportional to the total power in the wave, S_2 is the excess of power in the linear polarization along the x-direction over that in the y-direction, S_3 is the equivalent of S_2 with the references axes rotated through 45^o in the positive direction, and, finally, S_4 is the excess of the right circularly polarized power over that in the left.

The degree of polarization p is related to the extent to which the power in the wave can be separated into a single polarization. Numerically the degree of polarization is equal to the maximum of the ratio of the difference between the power in two orthogonal modes and the total power in the wave. Appendix A briefly shows that the degree of polarization according to this definition is given by:

$$p = \frac{1}{S_1} \sqrt{S_2^2 + S_3^2 + S_4^2} \tag{3}$$

which is also the usual definition (Born and Wolf, 1959, p. 551).

The wave in passing through a medium, or in being reflected or scattered from an interface will, in general, change its state of polarization and hence the various components of Stokes vector will be transformed. Such transformations may or may not alter the degree of polarization p.

The transformation of the four components of Stokes vector when the wave passes through a medium or is being scattered or reflected by a surface, may be described by a matrix M relating the Stokes vector before transformation, $\vec{S}$, to that after transformation, $\vec{S}'$, i.e.,

$$\vec{S}' = M \vec{S} \tag{4}$$

In the most general situation the matrix M (The Mueller matrix) will contain sixteen elements. In principle, therefore, we are required to determine from observations these sixteen elements as a function of angle of incidence in order to achieve a complete statistical description of the scattering properties of the lunar surface. In the following paragraphs we shall employ symmetry arguments and reciprocity relations to reduce considerably the number of unknowns to be determined experimentally in the case of lunar scattering.

Let us first perform a number of "Gedanken experimente" to make use of symmetry properties.

Suppose the lunar surface is illuminated either with a right or a left circularly polarized wave, i.e., $S = \{1, 0, 0, \pm 1\}$. Since we must expect the scattered power as well as the excess of linear polarization to be the same in the two situations, we have:

$$
\begin{aligned}
M_{11} + M_{14} &= M_{11} - M_{14} \qquad \text{i.e.,} \qquad M_{14} = 0 \\
M_{21} + M_{24} &= M_{21} - M_{24} \qquad \text{i.e.,} \qquad M_{24} = 0 \\
M_{31} + M_{34} &= M_{31} - M_{34} \qquad \text{i.e.,} \qquad M_{24} = 0
\end{aligned}
\tag{5}
$$

Furthermore, the amount of "circular depolarization" must be the same in the two cases. This means that:

$$
M_{41} + M_{44} = -(M_{41} - M_{44}) \qquad \text{i.e.,} \qquad M_{41} = 0 \tag{6}
$$

Reciprocity relations (Rumsey, 1954) also indicate that the power received in the y-component when transmitting waves linearly polarized along the x-direction is the same as the power received in the x-component when the same transmitted wave is polarized along the y-direction. Thus must apply for arbitrary choice of x and y directions, which means that:

$$
\begin{aligned}
M_{11} + M_{12} - M_{21} - M_{22} = M_{12} &= M_{12} + M_{21} - M_{22} \qquad \text{i.e.,} \quad M_{12} = M_{21} \\
M_{11} + M_{13} - M_{31} - M_{33} = M_{11} &- M_{13} + M_{31} - M_{33} \qquad \text{i.e.,} \quad M_{13} = M_{31}
\end{aligned}
\tag{7}
$$

Illumination of the moon with a linearly polarized wave cannot give rise to preferential circular polarization and hence one must have

$$
M_{42} = M_{43} = 0 \tag{8}
$$

To proceed further with these arguments we next orient the xy reference coordinate system with respect to the plane of incidence of the backscattering surface in such a way that the x-axis is in the plane of incidence. The Mueller matrix corresponding to this situation is denoted by M^o and its elements by M^o_{ij}.

In this situation we can argue that the same total power must be scattered back irrespective of whether the transmitted linear polarization makes an angle of $+45^o$ or -45^o with respect to the plane of incidence. This means that

$$M^o_{13} = M^o_{31} = 0 \tag{9}$$

The same two types of transmissions must give rise to identical values of S'_2 which means that

$$M^o_{23} = 0 \tag{10}$$

Transmission polarized linearly either in or across the plane of incidence for reasons of symmetry must give $S'_3 = 0$ which means that

$$M^o_{32} = 0 \tag{11}$$

For this particular choice of coordinate axes with respect to a scattering element one therefore obtains for M^o:

$$M^o = \begin{pmatrix} M^o_{11} & M^o_{12} & 0 & 0 \\ M^o_{12} & M^o_{22} & 0 & 0 \\ 0 & 0 & M^o_{33} & 0 \\ 0 & 0 & 0 & M^o_{44} \end{pmatrix} \tag{12}$$

The matrix elements for other orientations of the coordinate axes can be found from (12) by a simple coordinate rotation transformation, see Appendix B. In particular, we see from B5 that the average of M over angle ψ is:

$$\langle M \rangle_{\psi} \begin{pmatrix} M^{o}_{11} & 0 & 0 & 0 \\ 0 & \frac{1}{2}(M^{o}_{22} + M^{o}_{33}) & 0 & 0 \\ 0 & 0 & \frac{1}{2}(M^{o}_{22} + M^{o}_{33}) & 0 \\ 0 & 0 & 0 & M^{o}_{44} \end{pmatrix} \qquad (13)$$

Hence it may be concluded that a complete statistical description of the electromagnetic backscattering properties of the lunar surface at each frequency and angle of incidence requires the determination of five independent quantities.

3. Experimental Equipment

The antenna beam of the Millstone Hill radar system is somewhat wider than the angular extent of the moon. Resolution in range will single out areas where the incoming radiation has a constant angle of incidence, but in order to separate out small areas with a well defined direction of the plane of incidence as seen from the radar system, additional discrimination was required using Doppler resolution. Due to a slight apparent angular rotation of the moon as seen from the radar, different areas on the moon will have different doppler offsets with respect to that of the center of the lunar disk. Lines of constant doppler offset will be straight parallel lines across the disk of the moon. Regions with near-zero doppler offset correspond to areas where the local plane of incidence is near-parallel to lines of constant doppler offset. Areas of maximum doppler offset for a particular range ring, on the other hand, have their local plane of incidence normal to lines of constant doppler shift. For zero and maximum doppler offset the local plane of incidence of the area under study therefore corresponds to well defined directions with respect to the radar system. Range-doppler cells with intermediate doppler values correspond to a super-position of two areas on the moon with differently oriented planes of incidence and can, therefore, not so conveniently be employed in polarization studies.

Since the doppler axis is rotating quite rapidly with respect to the radar system even on an hourly basis it follows that polarization studies based on resolution by means of the range-doppler technique can only be carried out provided the feed polarization of the transmit and receive antennas can be adjusted rather freely and rapidly. Certain modifications, therefore, had to be made to the original Millstone tracking feed system to meet these requirements.

The original feed system could be excited in the right or the left circularly polarized modes by applying the transmitter power to one or the other of two input ports to the feed system. In order to produce an arbitrary polarization of the transmitted wave the power must be divided at will between these two ports and the relative phase of the two signals must be adjustable. The arrangement finally employed is shown schematically in Figure 1.

Phase changer Ph 2 controls the relative levels of the power at the input of the two antenna ports. Phase changer Ph 1 controls their relative phase. For circular polarization all the power is applied to one of the two antenna input ports; for linear polarization the power is divided equally between the two antenna ports by adjusting Ph 2. The plane of linear polarization is then set by adjusting Ph 1. Arbitrary elliptical polarizations can also be produced but were never used in the experiments to be described. All the adjustments described can be carried out during normal transmission conditions.

The modes of polarization received was controlled by a similar arrangement of phase changers and power splitters (hybrids) as that shown between the dotted lines in Figure 1. The input to the arrangement was derived from ports 1 and 2 of Figure 1. The receiver polarizations could, in principle, also be set up in the data processing procedure by properly combining the coherently detected in-phase and quadrature components of the signal. This requires the radio frequency amplifiers as well as the various mixers and intermediate frequency amplifiers to be stable in gain and phase and tests on the existing equipment showed that this was not the case to a degree required by the observations. By combining the two orthogonal received polarizations at radio frequencies — before passing the signal through any phase or gain-sensitive components — the two receiver chains essentially only act as power measuring devices.

The degree of circularity transmitted could be checked by rotating a linear receiving dipole on the center of the antenna beam a distance of 500 m. from the antenna. The ratio of maximum to minimum power received on the linear dipole was about 0.3 — 0.4 db. When setting the system up for linear polarization the maximum to minimum could easily be made better than 30 db. It turned out, however, that tests of the antenna in the receive mode showed that the two nominally orthogonal linear polarizations for some settings deviated from orthogonality by up to 5°. This in turn means that depolarization ratios smaller than some -18 db could not be measured.

The Haystack radar used to obtain some of the data reported on below at a wavelength of 3.8 cm is at the moment only equipped to transmit a circularly polarized wave. The insertion of a network similar to that shown in Figure 1, however, made it possible to receive either circularly polarized waves or an arbitrary pair of orthogonal linearly polarized waves.

4. Observations and Results

In this section the observational techniques and results are briefly described. The various types of observations are related to the matrix elements of equation (12) in order to ensure that a complete electromagnetic description of the scattering is achieved. The observations are described in terms of increasing complexity beginning with incoherent results, i.e., results where all the power from a complete ring of constant range is combined. Thereafter some observations are described in which the polarization of the receiving equipment is continuously changed so as to relate the receiver polarization to the doppler cells on the moon, and finally, an experiment is described in which both transmit and receive polarizations had to be changed continuously and independently in relation to lunar doppler cells.

4.1. Measurement of Circular Depolarization, Range Ring

Measurements of circular depolarization have been carried out previously and have been reported elsewhere (Evans and Hagfors, 1966) but the main results are, nevertheless, included briefly in the present paper for the sake of completeness.

Figure 2 shows the expected and the depolarized backscattered power plotted as a function of cos ϕ where ϕ is the angle of incidence. Both components have been corrected to account for the effect of the finite width of the polar diagram of the antenna. The two-way correction factor in db is plotted against cos ϕ in Figure 3. The relative gain of the two orthogonal channels was checked by means of a linearly polarized target transmitter and it was also checked by operating the radar system in a receiver mode as a radiometer with the moon as a thermal source. The two power gains were measured to be the same to within 10%. By gain ratio we here refer to the ratio of powers received in the two orthogonal modes at the point where the noise calibration pulse is inserted into the system when the antenna is illuminated by a plane unpolarized wave along the main beam.

From these results total power received – i.e., the sum of polarized and depolarized powers – was determined for each range and plotted against cosine of the angle of incidence in Figure 4. Also shown is the total power versus range curve for linearly polarized transmission. Reference will be made to this curve below. The ratio of the polarized and the depolarized components is plotted against the same abscissa in Figure 5. Knowing the total relative power as a function of range, the ratio of the depolarized and the polarized components and the cross section of the moon measured with the polarized component only (Evans and Hagfors, 1966) suffices to determine the Mueller matrix elements M_{11} and M_{44}, see (12). We shall return to actual numerical evaluations and discussions of possible models in Section 5.

4.2. Measurement of Linear Depolarization, Range Ring

The linear depolarization measurements were carried out by transmitting with a fixed, usually vertical polarization, In order to avoid difficulties with Faraday rotation the linear polarization at the receiver was rotated between runs. The output power in each polarization would therefore vary sinusoidally about a mean level proportional to $\frac{1}{2} M_{11}{}^{o}$ and with an amplitude proportional to

$\frac{1}{4}$ $(M^o_{22} + M^o_{33})$, see equation (13). The least mean square sinewave was fitted to the data and the mean and the depth of modulation was determined to give the total power and the power ratios. A correction for the polar diagram was made here as in the case of circular polarization, (see Figure 3). Figure 6 shows the polarized and the depolarized linear components again as a function of cos ϕ. Their ratio is shown in Figure 7. A comparison of these results with those obtained with circularly polarized waves will be made in Section 5. We only note here that this experiment provides direct information about the quantity $M^o_{22} + M^o_{33}$. The angular variation of M^o_{11} which was determined from the circularly polarized data, see Fig. 4, was also determined as a check from the linearly polarized data by summing the polarized and the depolarized components. The angular relationship is shown in Figure 4. Please note that the fact the two curves are displayed at different power levels does not reflect a difference in the two cross sections, only a difference in the calibration of the system during the two runs compared. The angular variation is seen to be closely similar.

4.3. Measurement of Power in Orthogonal Linear Polarizations for Circularly Polarized Illumination, Area Element

From (12) and (13) it can be seen that the quantity M^o_{12} can only be determined provided resolution is available in addition to that provided by range gating which was used exclusively to obtain the data described in the previous two subsections. In order to determine M^o_{12} or the difference of the backscattering coefficients for waves polarized in and across the local plane of incidence the moon was illuminated by a circularly polarized wave and the two receiver chains were adjusted so that one was sensitive to linearly polarized waves with direction of polarization parallel to the projected libration axis of the moon and the other perpendicular to this axis. Any variation in the backscattering coefficient with angle with respect to the local plane of incidence must show up in a difference in the frequency spectrum of the return for a particular range ring on the moon. For a more detailed description of the basic principles involved in this experiment the reader is referred to Hagfors et al (1965). Figure 8 shows a few normalized spectra for the two receiver polarizations. The normalization consists in forcing the two frequency spectra corresponding to the same range to have the same area, i.e., the same returned power. As can be seen, the component corresponding to E-field aligned with the libration axis is stronger than the other near zero frequency, but less strong than the other near maximum frequency for the range ring considered. The effect observed could in principle be obtained if the antenna beams for the two linear polarizations were different. Scans of the solar disk with the receivers used as radiometers were therefore made for both linear polarizations, the scans being carried out both in azimuth and in elevation. These tests showed that the polar diagrams were identical to within 5% at an angular separation from the center of the beam corresponding to the limb of the moon.

The ratio of the two backscattering coefficients was derived from curves such as those shown in Figure 8 and the ratio plotted against cos ϕ in Figure 9. This determines the matrix element M_{12}^{o} in (12). Note that the component which has its E-field in the local plane of incidence is the stronger one.

A series of lunar polarization experiments similar to those described so far for a wavelength of 23 cm have been begun at a wavelength of 3.8 cm and the equivalent of the experiment described under the present subsection has been carried out.

In the 3.8 cm experiment using the 36 meters diameter Haystack antenna the beamwidth is approximately only one tenth of the diameter of the lunar disk. The angular resolution necessary to define a local plane of incidence on the moon is, therefore, provided directly by the beam itself and by a range resolution capability. The experiment was in practice carried out by transmitting in the circularly polarized mode and by receiving two orthogonally polarized linear components. The antenna beam was moved out from the center of the lunar disk to the limb in steps along a radius of the disk and the polarization of the receiver channels was adjusted so that one was aligned with the radius and the other one was perpendicular to this radius. The center of the disk was used as a reference point where the backscattering coefficients for the two orthogonal polarizations by definition are equal. The results of the experiment are displayed in the form of a ratio of the power in the components polarized parallel and perpendicular to the local plane of incidence, in Figure 10 on the same scale as in Figure 9 for the 23 cm results.

4.4. Measurement of Power in Orthogonal Linear Polarizations for Linearly Polarized Illumination, Area Element.

The three basic types of experiments discussed so far still leave one quantity in (12) undetermined. Only the sum of M_{22} and M_{33} is known and it is necessary to determine either one of the two elements by an additional experiment.

The particular setup chosen to separate M_{22} and M_{33} in (12) consists in transmitting a linearly polarized wave in such a way that the direction of polarization is aligned with the direction of the instantaneous libration axis of the moon. The two orthogonally polarized receiver channels were aligned so that one corresponds to polarization in the local plane of incidence and the other normal to this plane. The experiment was carried out both by making use of the rotation technique at the receiver as described in subsection 4.2 and by actually aligning the receiver polarizations under conditions of low Faraday rotation. The results are shown in Figure 11 which displays the ratio of the two components as a function of cos ϕ. The comparatively large spread in the observed values is not completely understood. The most likely explanation is presently thought to be that local variations exist in the scattering properties of the lunar surface. It should be noted, however, that the amount of depolarization is less from a doppler strip than from a whole range ring when the illumination is linearly polarized parallel to this strip.

5. Discussion of Observational Results

The problem remains of relating the observed results to a reasonable model of the lunar surface. In this discussion we shall not be concerned with that part of the return which can be termed "quasispecular" and which may be well described in terms of a geometric optics model involving tilted smooth facets having mean slopes of the order of $10 - 12^{\circ}$ [Rea et al (1965); Hagfors (1965)]. In what follows our interest will primarily be focused on the part of the return which is caused by areas tilted by more than about 20° with respect to the direction of the incident radiation.

All data given above are relative; no absolute levels were established. Furthermore, the quasispecular return was not examined in great detail and in many cases was absent due to overloading. In order to compare the scattering from the lunar surface with scattering from other surfaces it was first necessary to establish the scattering cross section per unit lunar surface area. Previously the total lunar cross section at 23 cm was determined to be 0.065 ± 0.008 times the geometrical cross section. In general, let the radar cross section be a fraction R of the geometrical cross section, $P(\tau)$ the received power per unit delay, a the radius of the moon and c the speed of light. The scattering cross section σ per unit surface area then becomes:

$$\sigma = \frac{a \cdot R \cdot P(\tau)}{c\int P(\tau)d\tau} \tag{14}$$

This quantity was computed as a function of delay and angle of incidence from data presented elsewhere (Evans and Hagfors, 1966). The cross section per unit area was computed for 23 cm wavelength where the total cross section is quite accurately known, as well as for 3.8 and 68 cm where the total cross section is less accurately known and, therefore, was assumed to be the same as at 23 cm (see also Evans and Hagfors, 1966). The results are shown in Table 1. As can be seen there is a strong wavelength dependence in the quasispecular return near zero delay, the longer wavelengths being returned more strongly. At oblique angles of incidence, however, the wavelength dependence is much less pronounced and it is in the opposite direction, the shorter waves being scattered more strongly.

Extensive experimental studies of radar scattering from various types of rough surfaces have been carried out by Peake (1959). In particular, slightly rough asphalt and concrete surfaces were examined in great detail. The height deviation of the roughness was typically of the order of 0.01 times the wavelength and the horizontal scale was usually somewhat smaller than the wavelength. Dielectric constants were complex and of magnitude in the range 2.5 – 6.0. The amount of backscattering found by Peake was highly variable, depending on the autocorrelation function of the surface structure as well as on the intrinsic electrical properties of the surface material. Typical values of the backscattering coefficient per unit area found by Peake are, however, not drastically different from those found in lunar scattering. The angular variation of the backscattering also appears to be in general agreement with lunar results if an appropriate choice is made of roughness parameters either for asphalt or for concrete surfaces. Some of the surfaces discussed by Peake which are covered with certain types of vegetation also have similar backscattering cross sections. Since such a wide class

Table 1

Radar Cross Section per Unit Surface Area (db)

Delay (μsec)	∅ (deg)	3.8cm	23cm	68cm
10.	2.38	.83	2.77	4.29
20.	3.37	- 1.43	1.92	3.69
30.	4.12	- 1.98	1.37	2.79
40.	4.76	- 2.38	.87	2.09
50.	5.32	- 2.73	.42	1.49
60.	5.83	- 3.03	.02	.99
70.	6.30	- 3.33	-.38	.49
80.	6.73	- 3.58	-.78	-.01
90.	7.14	- 3.83	-1.18	-.51
100.	7.53	- 4.03	-1.53	-.91
125.	8.42	- 4.58	-2.28	-1.91
150.	9.22	- 5.03	-3.03	-2.71
175.	9.96	- 5.38	-3.68	-3.41
200.	10.65	- 5.73	-4.23	-4.11
225.	11.30	- 6.03	-4.73	-4.71
250.	11.92	- 6.33	-5.23	-5.41
275.	12.50	- 6.68	-5.68	-5.86
300.	13.06	- 6.93	-6.08	-6.41
325.	13.59	- 7.23	-6.43	-6.81
350.	14.11	- 7.48	-6.78	-7.31
375.	14.61	- 7.73	-7.13	-7.61
400.	15.09	- 7.98	-7.43	-8.06
425.	15.56	- 8.23	-7.73	-8.41
450.	16.01	- 8.43	-8.03	-8.71
475.	16.45	- 8.63	-8.43	-9.01
500.	16.88	- 8.78	-8.58	-9.31
600.	18.51	- 9.33	-9.53	-10.31
700.	20.01	- 9.83	-10.43	-11.11
800.	21.40	-10.23	-11.23	-11.91
900.	22.72	-10.63	-11.83	-12.61
1000.	23.97	-10.93	-12.58	-13.31
1100.	25.15	-11.08	-13.18	-13.96
1200.	26.29	-11.58	-13.63	-14.61
1300.	27.39	-11.83	-14.03	-15.21
1400.	28.44	-12.08	-14.38	-15.71
1500.	29.46	-12.33	-14.68	-16.11
1750.	31.88	-13.33	-15.88	-17.51
2000.	34.15	-13.73	-16.33	-18.01
2250.	36.29	-14.18	-16.78	-18.41
2500.	38.33	-14.58	-17.08	-18.81
2750.	40.28	-14.88	-17.43	-19.21
3000.	42.15	-15.23	-17.73	-19.51
3250.	43.96	-15.53	-18.08	-19.81
3500.	45.71	-15.83	-18.38	-20.01
3750.	47.41	-16.13	-18.63	-20.21
4000.	49.07	-16.38	-18.93	-20.41
4250.	50.68	-16.63	-19.18	-20.61
4500.	52.26	-16.93	-19.58	-20.81
4750.	53.81	-17.13	-19.73	-21.06
5000.	55.32	-17.43	-19.98	-21.31
5250.	56.81	-17.73	-20.28	-21.61
5500.	58.27	-17.98	-20.53	-21.86
5750.	59.71	-18.33	-20.83	-22.16
6000.	61.13	-18.63	-21.08	-22.51
6250.	62.53	-18.93	-21.43	-22.86
6500.	63.92	-19.33	-21.78	-23.21
6750.	65.29	-19.73	-22.18	-23.56
7000.	66.64	-20.13	-22.58	-23.96
7250.	67.98	-20.53	-23.03	-24.36
7500.	69.30	-21.03	-23.43	-24.71
7750.	70.62	-21.43	-23.88	-25.16
8000.	71.92	-21.88	-24.33	-25.66
8250.	73.21	-22.38	-24.83	-26.16
8500.	74.50	-22.88	-25.38	-26.66
8750.	75.78	-23.38	-25.93	-27.21
9000.	77.05	-23.98	-26.53	-27.81
9250.	78.31	-24.53	-27.18	-28.46
9500.	79.57	-25.33	-27.83	-29.06
9750.	80.82	-26.03	-28.58	-29.76
10000.	82.07	-26.93	-29.43	-30.61
10250.	83.32	-27.93	-30.48	-31.61
10500.	84.56	-29.33	-31.58	-32.61
10750.	85.80	-30.83	-33.08	-34.06
11000.	87.04	-32.03	-34.93	-35.81
11250.	88.27	-32.83	-37.58	-38.41

of surfaces exhibit approximately the same cross section it appears that the strength of the backscattering at oblique angles of incidence provides but a poor basis for determining the nature of the surface material on the moon.

Before proceeding to discuss the actual polarization data, let us consider the quasispecular reflection and what can be inferred from it. The strength of the quasispecular return is proportional to the power reflection coefficient at normal incidence. If the surface material is a homogeneous dielectric with dielectric constant ϵ (possibly complex) the reflectivity is given by

$$R = \left| \frac{\sqrt{\epsilon} - 1}{\sqrt{\epsilon} + 1} \right|^2 \tag{15}$$

and the magnitude of the dielectric constant may be determined.

Suppose we have a uniform upper layer with a dielectric constant ϵ_1 and of constant depth equal to b and that the supporting layer is semi-infinite and has a dielectric constant ϵ_2. The power reflection coefficient of such a double layer can be shown to be, assuming lossless dielectrics:

$$R = \frac{\epsilon_1(\sqrt{\epsilon_2} - 1)^2 - (\epsilon_1 - 1)(\epsilon_2 - \epsilon_1) \sin^2(\sqrt{\epsilon_1}\, kb)}{\epsilon_1(\sqrt{\epsilon_2} + 1)^2 - (\epsilon_1 - 1)(\epsilon_2 - \epsilon_1) \sin^2(\sqrt{\epsilon_1}\, kb)} \tag{16}$$

For a derivation the reader is referred to Sommerfeld's explanation of the colors displayed by an oildrop on wet asphalt (Sommerfeld, 1950). For the lunar surface we cannot expect the depth b of the top layer to be uniform. Instead we must expect the depths in the range b, b + db to occur with a certain probability p(b) db. The mean reflectivity at normal incidence must therefore be:

$$\langle R \rangle = \int_0^\infty p(b)\, R(b) \cdot db \tag{17}$$

where R(b) is given in Eq.(16). The actual average reflection coefficient will depend rather strongly on the form of the distribution function and on the mean depth. Only the limiting cases of small and large mean depths are independent of the form of the probability density p(b). For small mean depths, i.e., depth $< \lambda_o/4\sqrt{\epsilon_1}$ one obtains:

$$\langle R \rangle = \left(\frac{\sqrt{\epsilon_2} - 1}{\sqrt{\epsilon_2} + 1}\right)^2 \tag{18}$$

i.e., the top layer becomes invisible as one would expect. When the mean depth becomes large, the average reflection coefficient becomes:

$$\langle R \rangle = 1 - \frac{4\sqrt{\epsilon_1 \epsilon_2}}{(\sqrt{\epsilon_2} + 1)(\sqrt{\epsilon_2} + \sqrt{\epsilon_1})} \tag{19}$$

This reduces to Eq. (15) when $\epsilon_1 = \epsilon_2$ and when $\epsilon_1 = 1$ as it should. For a fixed value of ϵ_2 the average reflection coefficient has a minimum when $\epsilon_1 = \sqrt{\epsilon_2}$ which is the familiar relationship used when optical surfaces are given a dielectric coating to reduce reflections. Figure 12 shows some results of numerical evaluations of Eq. (19) for various combinations of ϵ_1 and ϵ_2. As can be seen the presence of a tenuous surface layer can reduce the reflectivity quite appreciably with respect to the reflectivity in the absence of a surface layer. Note that an increase in wavelength might bring about a gradual transition from a region where Eq. (18) applies to one where Eq. (19) applies, and a two-layer model could hence explain a wavelength dependence in the cross section.

Even more complex models for reflection at normal angles of incidence have been suggested; in particular one involving a gradual linear transition from vacuum to some relatively high value whereupon the dielectric constant remains constant with depth (Giraud, 1965). Figure 13 shows a slightly more general model in that a jump in dielectric constant is allowed at the vacuum-material interface. Again assuming lossless dielectrics the reflection coefficient at normal incidence becomes:

$$R = \left| \frac{\text{Det-}}{\text{Det+}} \right|^2 \tag{20}$$

where

$$\text{Det} \pm = \left\{S_B \left(\frac{\alpha b \epsilon_1}{\Delta\epsilon}\right) \pm \frac{i\alpha}{k} S_B' \left(\frac{\alpha b \cdot \epsilon_1}{\Delta\epsilon}\right)\right\} \left\{S_A \left(\frac{\alpha b \epsilon_2}{\Delta\epsilon}\right) - \frac{i\alpha}{k\sqrt{\epsilon_2}} S_A' \left(\frac{\alpha b \epsilon_1}{\Delta\epsilon}\right)\right\} -$$

$$- \left\{S_A \left(\frac{\alpha b \epsilon_1}{\Delta\epsilon}\right) \pm \frac{i\alpha}{k} S_A' \left(\frac{\alpha b \epsilon_1}{\Delta\epsilon}\right)\right\} \left\{S_B \left(\frac{\alpha b \epsilon_2}{\Delta\epsilon}\right) - \frac{i\alpha}{k\sqrt{\epsilon_2}} S_B' \left(\frac{\alpha b \epsilon_1}{\Delta\epsilon}\right)\right\} \quad \ldots\ldots \quad (21)$$

where

$$\alpha = (k^2 \Delta\epsilon/b)^{1/3}$$

$$\Delta\epsilon = \epsilon_2 - \epsilon_1$$

and where S_A and S_B are any two independent solutions of Stokes differential equation. Figure 14 shows an example of reflectivity R plotted against the ratio of transition layer thickness and wavelength for $\epsilon_2 = 4.0$ and for several values of ϵ_1. The case $\epsilon_1 = 1.0$ corresponds to Giraud's case (Giraud, 1965). As can be seen the linear gradient introduces a "match" between vacuum and the underlying layer even for very moderate layer thickness. For layers deeper than about one half the wavelength essentially only the initial jump in ϵ, i.e., $\epsilon_1 - 1$ gives rise to reflection. In the case $\epsilon - 1 = 0$ the reflectivity should approach zero and not the constant value quoted by Giraud. It is not clear how this discrepancy was brought about. Most likely it may stem from an erroneous application of the phase integral method as opposed to the exact method leading to equation (21).

From the discussion of these examples it is obvious that a number of surface models can be constructed which may account for the strength of the quasi-specular component of the returned echo and even the frequency dependence of the return.

Let us next turn to the question of interpreting the various kinds of polarization observations.

The depolarization of circularly polarized scattered waves for circularly polarized illumination may be thought of as arising in at least one of two different ways. There may either be a systematic difference in the backscattering coefficients for waves polarized in or perpendicular to the local plane of incidence (the two principal linear polarizations). There may also be a depolarization of the two principal linearly polarized waves in the sense that illumination in one principal linear polarization gives rise to scattered power in the orthogonal linear polarization also. The results of Section 4.3 of this paper show that the former of the two possibilities does occur. On the other hand, the results of Section 4.4 show that the latter type of mechanism is also present. In order to evaluate the relative importance of these mechanisms in causing depolarization of circularly polarized waves one may argue as follows.

Let the backscattering matrix of a surface element be:

$$S = \begin{Bmatrix} r_{11} & r_{12} \\ r_{21} & r_{22} \end{Bmatrix} \tag{22}$$

so that the linearly polarized fields in and across the local plane of incidence, E_1 and E_2, respectively, are related to the incident fields E_1' and E_2' through:

$$\begin{Bmatrix} E_1 \\ E_2 \end{Bmatrix} = \begin{Bmatrix} r_{11} & r_{12} \\ r_{21} & r_{22} \end{Bmatrix} \begin{Bmatrix} E_1' \\ E_2' \end{Bmatrix} \tag{23}$$

The corresponding connection between circularly polarized waves is:

$$\begin{Bmatrix} E_r \\ E_\ell \end{Bmatrix} = \frac{1}{2} \begin{Bmatrix} r_{11} + r_{22} - i\,(r_{12} - r_{21}) \,, & r_{11} - r_{22} - i\,(r_{12} + r_{21}) \\ r_{11} - r_{22} + i\,(r_{12} + r_{21}) \,, & r_{11} + r_{22} + i\,(r_{12} - r_{21}) \end{Bmatrix} \begin{Bmatrix} E_r' \\ E_\ell' \end{Bmatrix}$$

The ratio of depolarized to polarized circular when the illumination is circular hence becomes:

$$\frac{\text{Depol}}{\text{Pol}} = \frac{\langle |r_{11} - r_{22} - i\,(r_{12} + r_{21})|^2 \rangle}{\langle |r_{11} + r_{22} + i\,(r_{12} - r_{21})|^2 \rangle} \tag{24}$$

In the particular case when $r_{12} = r_{21} = 0$, one obtains:

$$\frac{\text{Depol}}{\text{Pol}} = \frac{\langle |r_{11} - r_{22}|^2 \rangle}{\langle |r_{11} + r_{22}|^2 \rangle} \tag{25}$$

If the phases of the two reflection coefficients are the same the circular depolarized to polarized power ratio may be expressed directly in terms of the ratio of the two principal linear power backscattering coefficients $\rho_{||}$ and $\rho_{\perp}$ as follows:

$$\frac{\text{Depol}}{\text{Pol}} = \left(\frac{\sqrt{\rho_{||}} - \sqrt{\rho_{\perp}}}{\sqrt{\rho_{||}} + \sqrt{\rho_{\perp}}} \right)^2 \tag{26}$$

Figure 15 shows a plot of the expected ratio of depolarized and polarized power for circular polarization as a function of the ratio $\rho_{||}/\rho_{\perp}$. Note that in this case there would be no depolarization of the two principal linearly polarized components. We also note that a systematic phase difference of the two reflection coefficients $\rho_{||}$ and $\rho_{\perp}$ would lead to a preferential circular polarization of the scattered wave for linearly polarized illumination. This possibility was excluded at the outset of our discussion as being physically implausible.

Figure 15 shows that the difference in the reflection coefficients $\rho_{||}$ and $\rho_{\perp}$ actually observed, see Figure 9, is inadequate to account for the depolarization of circularly polarized waves. It is therefore concluded that r_{12} and r_{21} being nonzero as indicated by the observational results shown in Figure 11 must also be an important factor in producing depolarization.

In order to continue the discussion it is convenient at this point to introduce a specific model mechanism which may be adjusted to reproduce the observed data. Imagine that the backscattering in part arises from specular reflectors which do not depolarize at all. This type of mechanism clearly is dominant near the subradar point as indicated by the data presented. With increasing angles of incidence we imagine the scattering to occur increasingly from a discrete structure which acts as single scatterers. — These discrete scatterers may, as a first approximation, be thought of as linear dipoles of more or less random orientation. The assumption of single scattering rather than multiple scattering to account for the polarization effects is justified by the very low reflectivity of the lunar surface material.

A linear dipole will depolarize a circularly polarized wave completely, i.e., the energy scattered in right and left polarizations will be of equal strength. By observing the ratio of depolarized to polarized power as above it is therefore possible to estimate the relative amount of power P_r scattered by the reflection mechanism and the power P_S by the dipole scatter mechanism. The ratio of depolarized to polarized power becomes:

$$\frac{\text{Depol}}{\text{Pol}} = \frac{\frac{1}{2} P_S}{P_r + \frac{1}{2} P_S} \tag{27}$$

Figure 16 shows the ratio of depolarized to polarized power plotted as a function of the ratio of power scattered by dipoles to total scattered power. Comparison of the results in Figure 2 with the curve in Figure 16 shows that 70% of the power returned at oblique angles of incidence is to be ascribed to the dipole scattering mechanism. A collection of randomly oriented dipoles illuminated with a linearly polarized wave will return 25% of the scattered power in the orthogonal mode. In this case, therefore, the ratio of depolarized to polarized power for circularly polarized waves becomes:

$$\frac{\text{Depol}}{\text{Pol}} = \frac{\frac{1}{4} P_S}{P_r + \frac{3}{4} P_S} \tag{28}$$

In Figure 17 this polarization ratio is plotted as a function of the fraction of the total power scattered by dipoles. Comparison with Figure 7 shows that again the fraction of the total scattered power which must be ascribed to the dipoles is in the vicinity of 70%.

This somewhat naive model of the scattering mechanism is so far unable to account for a preferential backscattering when the E-field is in the plane of incidence, as shown by the observational results of Figures 9 and 11. At least two modifications may be made to the model to accommodate this effect. It may be that the dipoles behave as if oriented preferentially in the vertical direction on the lunar surface. An alternative model was suggested by Hagfors et al (1965) in the form of a tenuous layer covering the dipoles. The preferential scattering of waves with E-field in the plane of incidence was explained as a preferential transmission of these waves through the tenuous top layer. The latter model requires that a large fraction of the scattering dipoles are buried underneath the tenuous layer. This assumption does, unfortunately, not appear to be in agreement with the recent Surveyor I pictures if these pictures are representative of the lunar surface in general. The pictures reveal large numbers of rocks on the surface. These rocks may well serve as the discrete scatterers which so conveniently accounts for most of the radar data. However, if the rocks are identical with the dipoles, it means that the scattering structure is not buried under a tenuous layer. Let us first examine whether the rocks actually seen in the Surveyor I pictures are numerous enough to account for the total scattered power at oblique angles of incidence. – The Surveyor pictures appear to indicate that the cumulative rock distribution is of the form:*

$$N = 3 \cdot 10^5 \cdot y^{-1.77} \tag{29}$$

where N = cumulative number of grains per 100 m^2

y = diameter of grains in mm.

The number density of rocks or grains per m^2 with diameter between y and $y + dy$ is:

$$n(y)\, dy = 5.31 \cdot 10^3 \cdot y^{-2.77} \tag{30}$$

The geometric cross section of each grain expressed in m^2 is:

$$\sigma_g = \frac{\pi}{4} y^2 \cdot 10^{-6} \tag{31}$$

---

*"Surveyor I, A Preliminary Report," Report SP-126, National Aeronautics and Space Administration (June, 1966).

Let us next assume that each grain scatters back with radar cross section which is a certain constant fraction R of its geometrical cross section when the diameter exceeds the wavelength and zero otherwise. The cross section per unit area is therefore found to be:

$$\sigma \approx \frac{\pi R}{4} \cdot 5.31 \cdot 10^{-3} \cdot \frac{1}{0.23} \left(y_{max}^{0.23} - y_{min}^{0.23} \right) \tag{32}$$

The distribution (29) emphasizes larger rocks, i.e., the larger rocks obscure more of the surface area than the smaller ones. For this reason one must assume, somewhat arbitrarily, a value for y_{max}. The cross section σ, however, is not very critically dependent on this choice. If we put y_{max} = 1000 mm we obtain, for λ = 23 cm

$$\sigma \approx R \cdot 0.083 \tag{33}$$

If the reflectivity of the grains is the same as for the moon as a whole we therefore obtain as a typical number for cross section per unit area:

$$\sigma \approx -23 \text{ db}.$$

This number is large enough to account for all the scattering at oblique angles of incidence, compare with the data of Table 1. Hence, if the Flamsteed area where Surveyor I landed is typical of the lunar surface the earlier interpretation of the radar data in terms of buried single scatterers (Hagfors, et al, 1965) must be rejected on the grounds that the scatterers as seen photographically rest on top of the surface rather than inside it. The presence of grains and rocks on top of the surface rather than buried inside the surface material does, however, not rule out the presence of a double layer surface model. It only means that the back-scattering at oblique angles of incidence takes place without appreciable penetration of the top layer. The double layer model is still attractive in certain respects both to explain a wavelength dependence of the quasispecular return as well as to account for the somewhat lower dielectric constant of the lunar surface material generally deduced by radiometer observations of thermal emission from the moon (Soboleva, 1962; Heiles and Drake, 1963; Baars et al, 1965; Davies and Gardner, 1966). Rather than having inhomogeniety in depth Davies and Gardner have constructed a model having lateral inhomogeniety. Their model of the lunar surface consists of 65 percent area with $\epsilon = 1.6$ and 35 percent with $\epsilon = 5.0$.

Local variations in the radar depolarizing properties of the lunar surface have so far not been studied extensively. The only information regarding local variability was reported by Hagfors et al (1965) and shows certain peculiarities in relation to the scattering from the crater Tycho. Several other craters have also been shown to be extraordinarily strong radar scatterers (Thompson, 1965), but detailed studies of their depolarizing properties have so far not been attempted.

The model of the lunar surface emerging from the present and past radar studies interpreted for compatibility with radiometric thermal emission data as well as with photographic close-up pictures appears to be as follows. The major portion of the surface is gently undulating with r.m.s. slopes on the order of $10 - 12^{\circ}$. This surface must be either horizontally or vertically inhomogeneous in order to reconcile radar and radiometric data. The depolarizing properties as observed in backscattering at oblique angles of incidence appears to be adequately explained by pebbles and rocks strewn over the smooth surface.

ACKNOWLEDGMENT

Illuminating discussions with Drs. J. V. Evans and G. H. Pettengill are gratefully acknowledged. The author is indebted to the personnel at the Millstone Hill Radar Station for enthusiastic support. The use of the facilities of the Lincoln Laboratory Millstone/Haystack complex, provided by the U.S. Air Force, is gratefully acknowledged.

TH/sk
14 October 1966

Appendix A

Let an arbitrary pair of two-dimensional orthogonal unit vectors be given in terms of $\vec{e}_x$ and $\vec{e}_y$ by:

$$\begin{aligned} \vec{e}_1 &= \alpha\vec{e}_x + \beta\vec{e}_y \\ \vec{e}_2 &= -\beta^*\vec{e}_x + \alpha^*\vec{e}_y \end{aligned} \tag{A1}$$

The components of the complex field along these directions are:

$$\begin{aligned} E_1 &= (\vec{e}_1 \cdot \vec{E}) \\ E_2 &= (\vec{e}_2 \cdot \vec{E}) \end{aligned} \tag{A2}$$

The difference in the power in these two orthogonal modes is:

$$\begin{aligned} \langle | E_1 |^2 \rangle - \langle | E_2 |^2 \rangle = S_2 (|\alpha|^2 - |\beta|^2) + S_3(\alpha\beta^* + \alpha^*\beta) + \\ + S_4(\alpha\beta^* - \alpha^*\beta)(-i) \end{aligned} \tag{A3}$$

By Schwartz inequality:

$$\left[\langle | E_1 |^2 \rangle - \langle | E_2 |^2 \rangle\right]^2 \leq \left(S_2^2 + S_3^2 + S_4^2\right)\left(|\alpha|^2 + |\beta|^2\right)^2 \tag{A4}$$

But from (A1) it follows that $|\alpha|^2 + |\beta|^2 = 1$, and the well known definition of degree of polarization (3) is therefore seen to be physically reasonable.

Appendix B

Rotation of the coordinate system through an angle ψ causes the components of a vector $\vec{E}$ to transform according to the rule:

$$\begin{Bmatrix} E_{x\psi} \\ E_{y\psi} \end{Bmatrix} = \begin{Bmatrix} \cos\psi & \sin\psi \\ -\sin\psi & \cos\psi \end{Bmatrix} \begin{Bmatrix} E_x \\ E_y \end{Bmatrix} \tag{B1}$$

The corresponding transformation of the Stokes vector can be found by simple substitution to be:

$$\begin{Bmatrix} S_{1\psi} \\ S_{2\psi} \\ S_{3\psi} \\ S_{4\psi} \end{Bmatrix} = \begin{Bmatrix} 1 & 0 & 0 & 0 \\ 0 & \cos 2\psi & \cos 2\psi & 0 \\ 0 & -\sin 2\psi & \cos 2\psi & 0 \\ 0 & 0 & 0 & 1 \end{Bmatrix} \begin{Bmatrix} S_1 \\ S_2 \\ S_3 \\ S_4 \end{Bmatrix} \tag{B2}$$

or abbreviated:

$$\vec{S}_\psi = T\,\vec{S} \tag{B3}$$

The Mueller matrix in the rotated coordinate system is:

$$M_\psi = T\,M\,\tilde{T} \tag{B4}$$

where $\tilde{T}$ is the transpose of T. Measuring ψ relative to the plane of incidence of the scattering element we obtain in general:

$$M_\psi = \begin{Bmatrix} M^o_{11}\ ; & M^o_{12}\cos 2\psi\ ; & -M^o_{12}\sin 2\psi\ ; & \\ M^o_{12}\cos 2\psi ; & M^o_{22}\cos^2 2\psi + M^o_{33}\sin^2 2\psi\ ; & (M^o_{33} - M^o_{22})\sin 2\psi\cos^2\psi ; & 0 \\ -M^o_{12}\sin 2\psi ; & (M^o_{33} - M^o_{22})\sin 2\psi\cos 2\psi\ ; & M^o_{33}\cos^2 2\psi + M^o_{22}\sin^2 2\psi ; & 0 \\ 0\ ; & 0\ ; & 0\ ; & M_{44} \end{Bmatrix}$$

(B5)

References

Baars, J. W. M., Mezger, P. G., Savin, N. and Wendker, H., "The Polarization of the Thermal Radiation of the Moon at 14.5 GHz", paper presented at 117th Meeting of the American Astron. Soc., 28-31 December 1964, Montreal, Canada.

Beckmann, P., "Radar Backscatter from the Surface of the Moon," J. Geophys. Research 70, 2345-2350 (1965a).

__________, "Shadowing of Random Rough Surfaces," IEEE Trans. Antennas Propag. AP-13, 384-388 (1965b).

Beckmann, P., and Klemperer, W. K., "Interpretation of the Angular Dependence of Backscattering from the Moon and Venus," J. Research Natl. Bur. Standards 69D, 1669-1677 (1965).

Beckmann, P., and Spizzichino, A., The Scattering of Electromagnetic Waves from Rough Surfaces (Macmillan, New York, 1963).

Born, M., and Wolf, W., Principles of Optics (Pergamon Press, New York, 1959).

Daniels, F. B., "Radar Determination of the Root Mean Square Slope of the Lunar Surface," J. Geophys. Research 68, 449-453 (1963).

Davies, R. D., and F. F. Gardner, "Linear Polarization of the Moon at 6, 11 and 21 cm Wavelength," Private communication (1966).

Davis, J. R., and Rohlfs, D. C., "Lunar Radio-Reflection Properties at Decameter Wavelengths," J. Geophys. Resdarch 69, 3257-3262 (1964).

Evans, J. V., "Radio-Echo Observations of the Moon at 3.6-cm Wavelength," Technical Report 256, Lincoln Laboratory, M.I.T. (19 February 1962), DDC 274669.

Evans, J. V., and Hagfors, T., "On the Interpretation of Radar Reflections from the Moon," Icarus 3, 151-160 (1964).

__________________, "Radio Echo Studies of the Moon at 23 cm. Wavelength," accepted for publication in J. Geophys. Research (1966).

Evans, J. V., and Pettengill, G. H., "The Radar Cross-Section of the Moon," J. Geophys. Research 68, 5098-5099 (1963a).

________________, "The Scattering Behavior of the Moon at Wavelengths of 3.6, 68 and 784 Centimeters," J. Geophys. Research 68, 423-447 (1963b).

Giraud, A., "Note on the Radio Reflectivity of the Lunar Surface," J. Research Natl. Bur. Standards 69D, 1677-1681 (1965).

Hagfors, T., "Some Properties of Radio Waves Reflected from the Moon and Their Relation to the Lunar Surface," J. Geophys. Research 66, 777-785 (1961).

Hagfors, T., "Relationship of Geometric Optics and the Autocorrelation Approaches to the Analysis of Lunar and Planetary Radar", J. Geophys. Research 71, 379-383, (1966).

Hagfors, T., Brockelman, R. A., Danforth, H. H., Hanson, L. B., and Hyde, G. M., "Tenuous Surface Layer on the Moon: Evidence Derived from Radar Observations," Science 150, 1153-1156 (1965).

Heiles, C. E., and Drake, F. D., "The Polarization and Intensity of Thermal Radiation from a Planetary Surface," Icarus 2, 281-292 (1963).

Peake, W. P., "The Interaction of Electromagnetic Waves with Some Natural Surfaces," Report 898-2, Ohio State University Research Foundation (30 May 1959).

Pettengill, G. H., and Henry, J. C., "Enhancement of Radar Reflectivity Associated with the Lunar Crater Tycho," J. Geophys. Research 67, 4881-4885 (1962).

Rea, R. D., Hetherington, N., and Mifflin, R., "The Analysis of Radar Echoes from the Moon," J. Geophys. Research 69, 5217-5223 (1964).

Rice, S. O., "Reflection of Electromagnetic Waves from Slightly Rough Surfaces," in The Theory of Electromagnetic Waves, (Interscience, New York, 1951), pp. 351-378.

Rumsey, V. H., "The Reaction Concept in Electromagnetic Theory," Phys. Rev. 94, 1483-1491 (1954).

Soboleva, N. S., "Measurement of the Polarization of Lunar Radio Emission on a Wavelength of 3.2 cm," Astron. J. USSR 39, 1124-1126 (1962).

Sommerfeld, A., Optik (Dieterich'sche Verlagsbuchhandlung, Wiesbaden, 1950) p. 43.

Thompson, T. W., "Lunar Mapping by Coherent Pulse Analysis," Radio Science 69D, 1667-1669 (1965).

Figure Legends

Figure 1. Arrangement for the control of polarization of the transmitted radiation.

Figure 2. Plot of the polarized and depolarized circular components for circular polarization transmitted. Power in decibels against cos ϕ, ϕ being angle of incidence.

Figure 3. Two-way antenna correction factor in decibels plotted against cos ϕ.

Figure 4. Plots of total returned power per unit area against cos ϕ, both for circular and for linear illumination. The difference in power levels of the two curves does not reflect a difference in cross section, only a difference in the system calibration during the two runs.

Figure 5. Ratio of polarized and depolarized components against cos ϕ, circular polarization.

Figure 6. Plot of polarized and depolarized components against cos ϕ, for linearly polarized illumination.

Figure 7. Ratio of polarized and depolarized components against cos ϕ, linear polarization.

Figure 8. Frequency spectra for the two linearly polarized received components for circularly polarized illumination.

Figure 9. Ratio of backscattered power in two orthogonal linearly polarized components for circularly polarized illumination.

Figure 10. Ratio of backscattered power in two orthogonal linearly polarized components for circularly polarized illumination, at 3.8 cm wavelength.

Figure 11. Ratio of backscattered power in two orthogonal linearly polarized components for linearly polarized illumination, polarization || of incidence. Dotted curve shows depolarization when polarization of illumination is averaged over all angles — for the same data.

Figure 12. Reflectivity of double layer of random thickness for various combinations of dielectric constant of upper layer ϵ_1 and of lower layer ϵ_2.

Figure 13. Surface model involving linear gradient in dielectric constant.

Figure 14. Reflection coefficient for dielectric double layer with linear gradient.

Figure 15. Plot of ratio of polarized and depolarized power for circularly polarized illumination as a function of the ratio of the back-scattering coefficients of the two principal linear polarizations.

Figure 16. Plot of ratio of polarized and depolarized power for circular illumination as a function of the fraction of power scattered by dipoles.

Figure 17. Plot of ratio of polarized and depolarized power for linear illumination plotted as a function of the fraction of power scattered by dipoles.

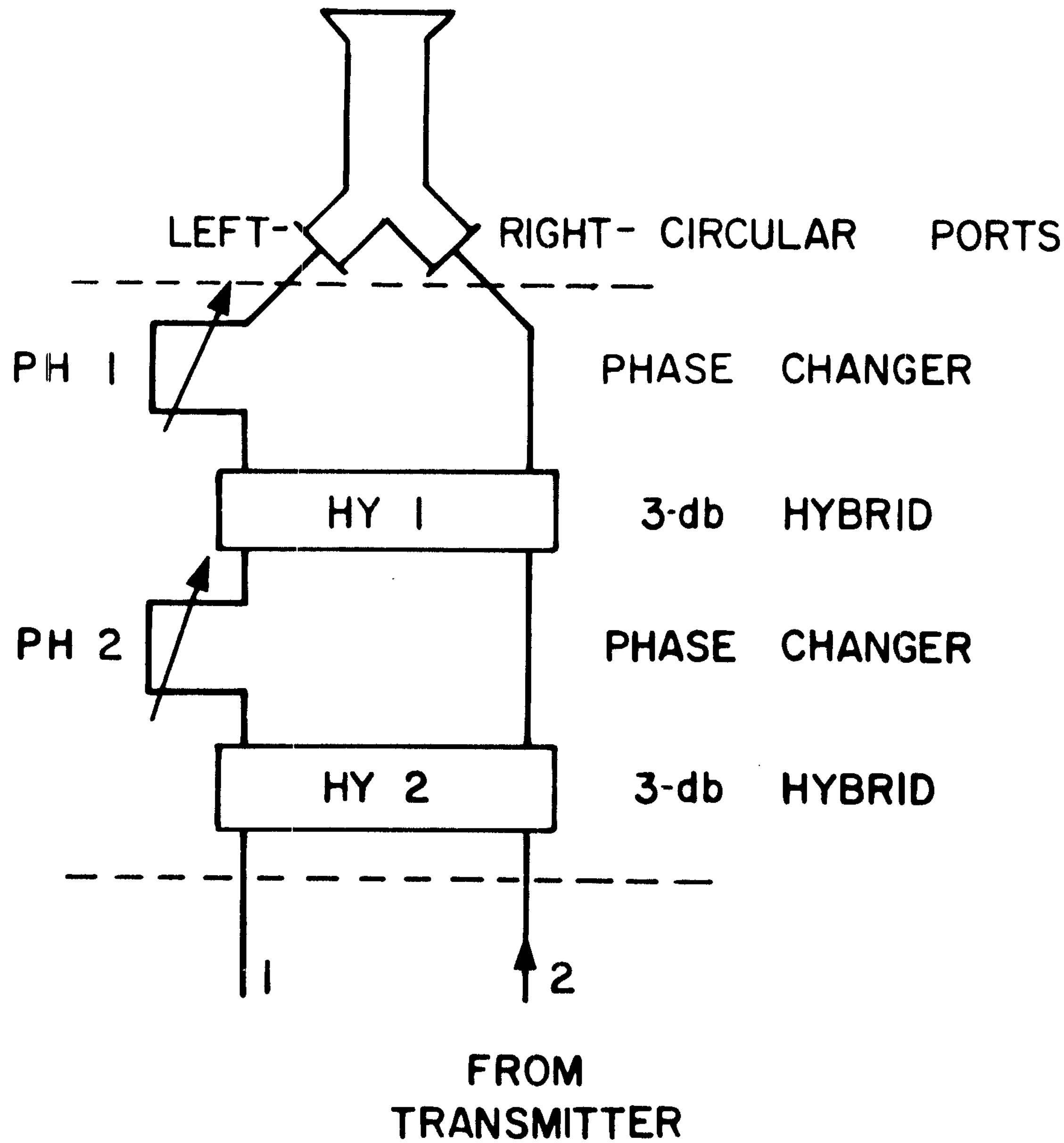

LEFT-
RIGHT- CIRCULAR PORTS
PH 1
PHASE CHANGER
HY 1
3-db HYBRID
PH 2
PHASE CHANGER
HY 2
3-db HYBRID
1
2
FROM TRANSMITTER

Fig. 1

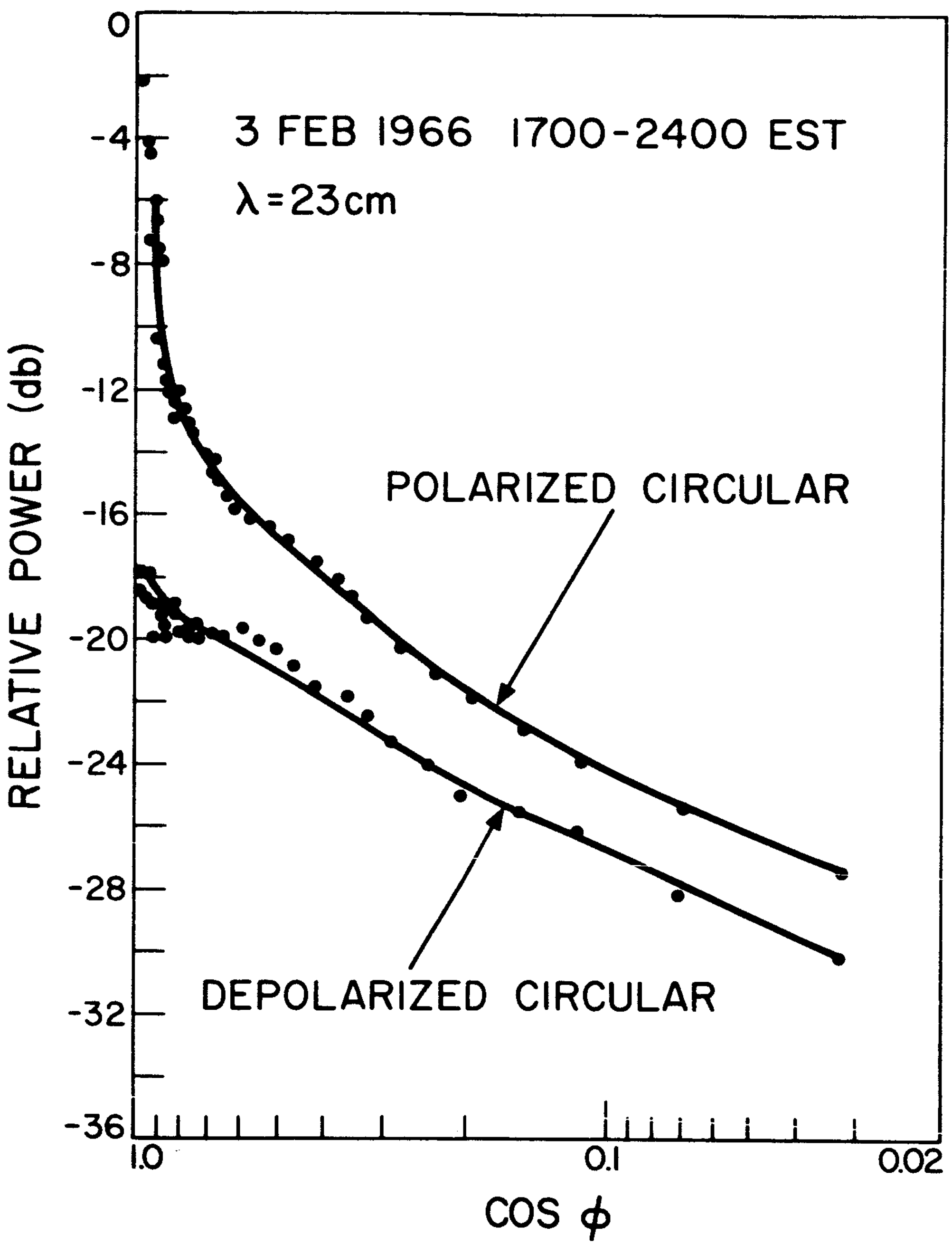

CIRCULAR TRANSMITTED AND RECEIVED

Fig. 2

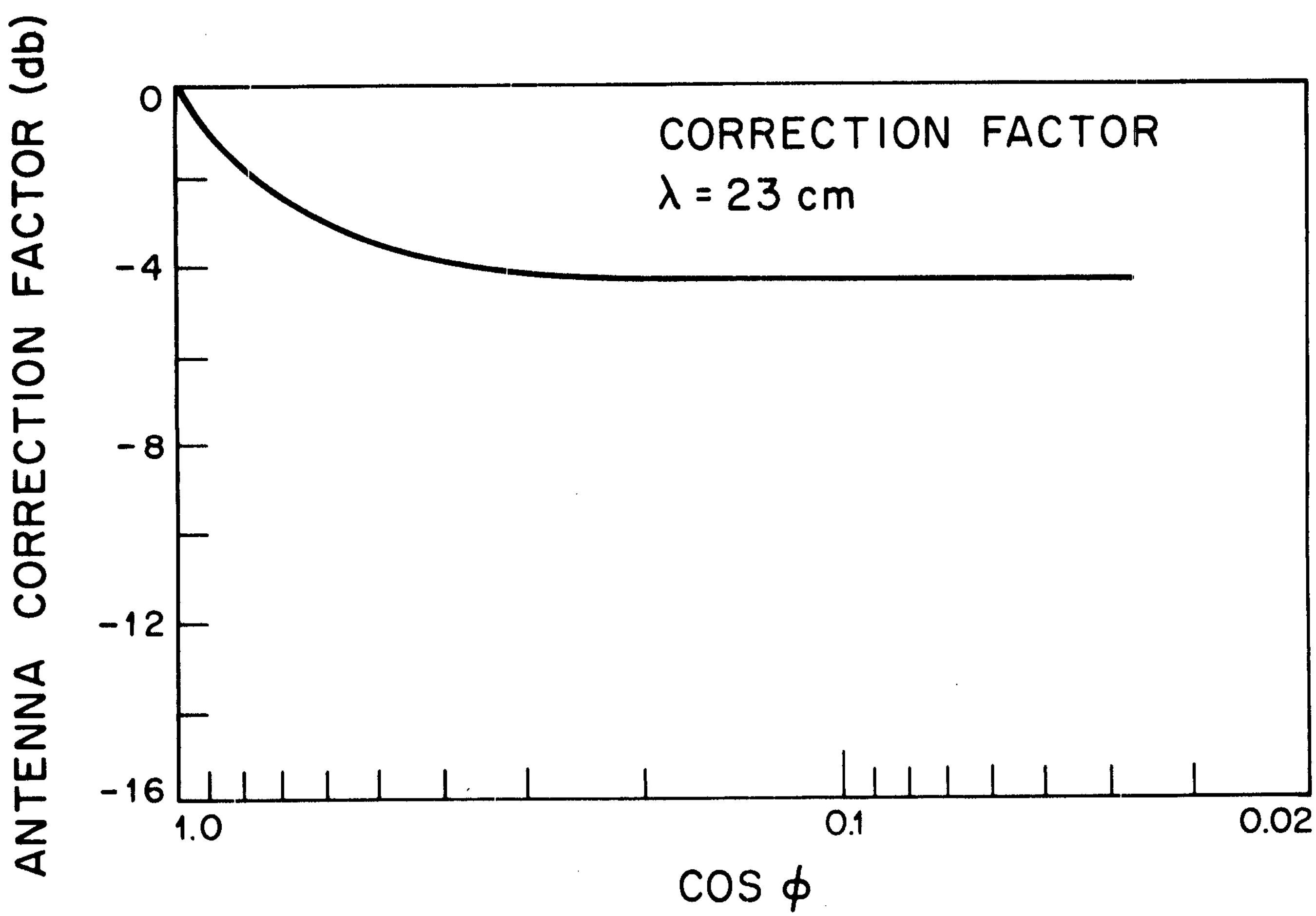

MILLSTONE ANTENNA PATTERN

Fig. 3

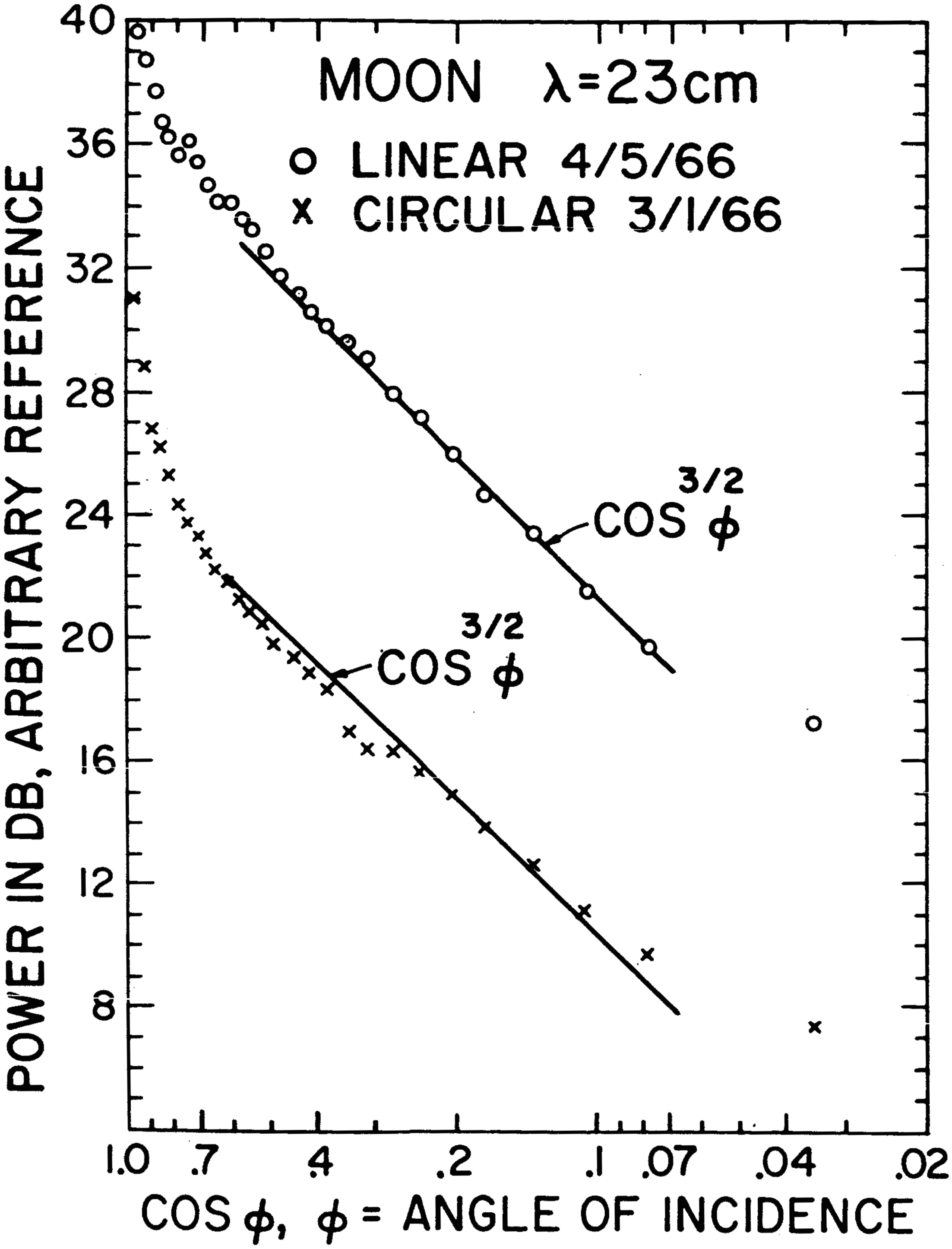
MOON λ=23cm
o LINEAR 4/5/66
x CIRCULAR 3/1/66
COS 3/2 φ
COS 3/2 φ
POWER IN DB, ARBITRARY REFERENCE
40
36
32
28
24
20
16
12
8
1.0
.7
.4
.2
.1
.07
.04
.02
COS φ, φ = ANGLE OF INCIDENCE

Fig. 4

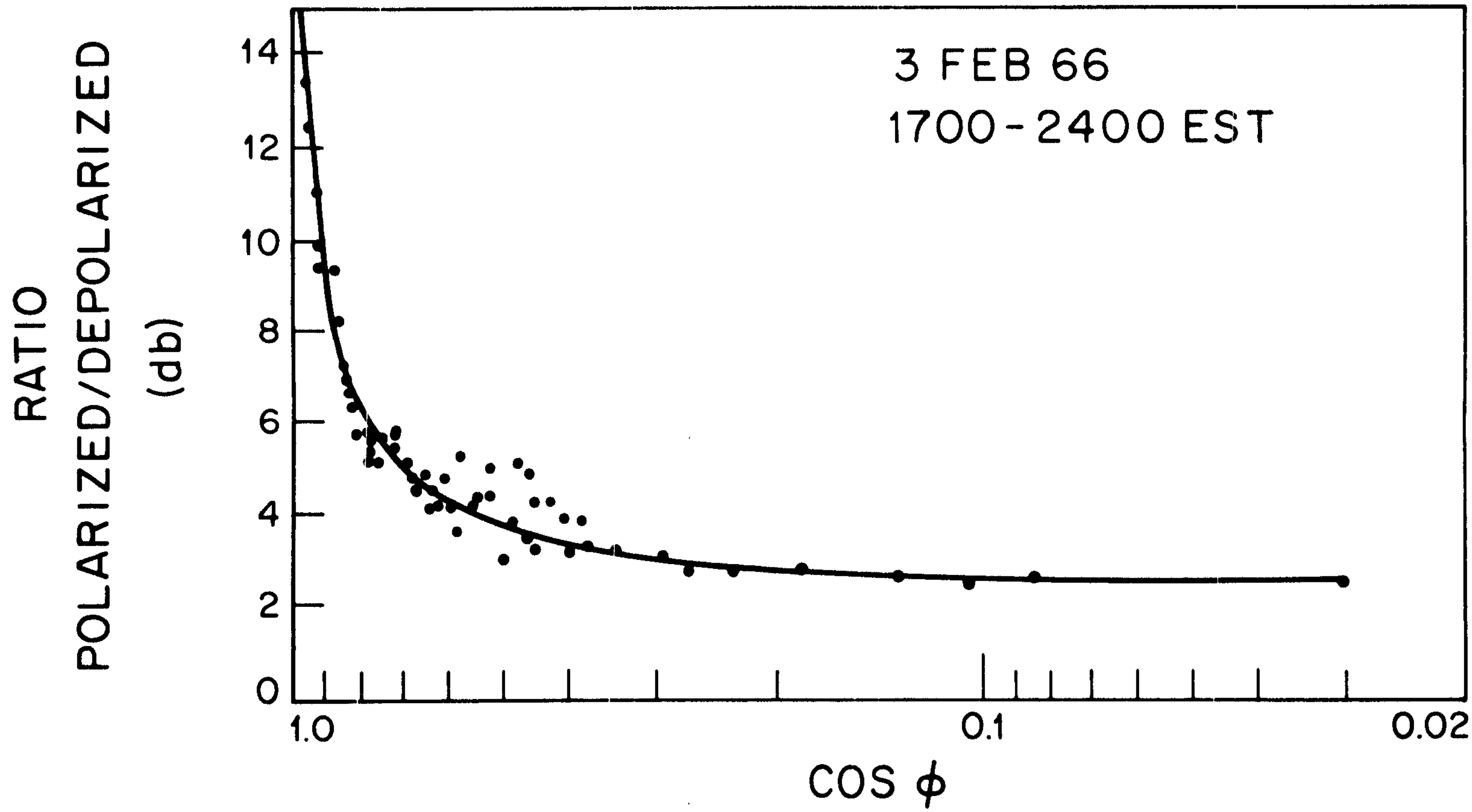

CIRCULAR ILLUMINATION

Fig. 5

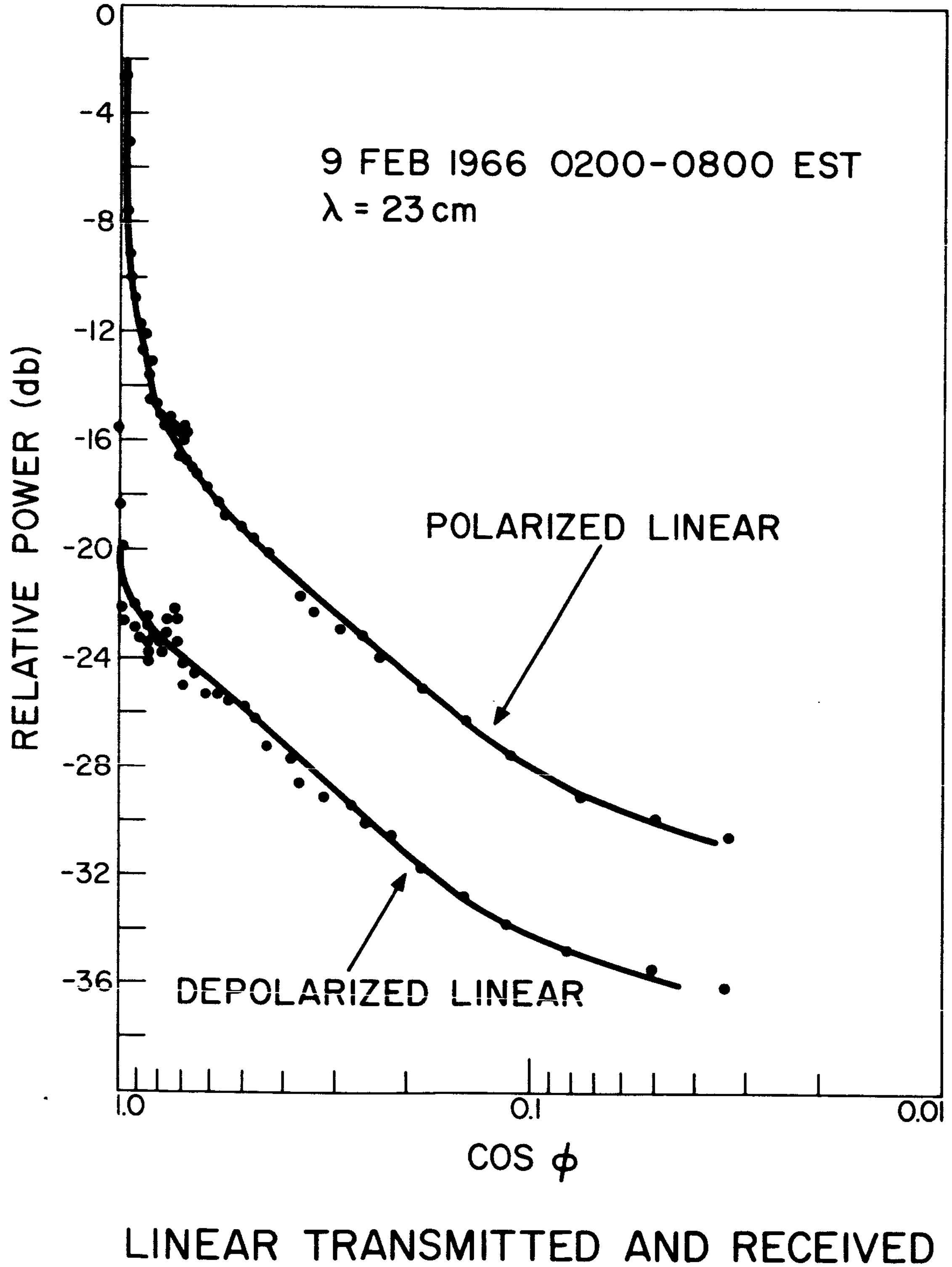

9 FEB 1966 0200-0800 EST
λ = 23 cm
POLARIZED LINEAR
DEPOLARIZED LINEAR
RELATIVE POWER (db)
0
-4
-8
-12
-16
-20
-24
-28
-32
-36
1.0
0.1
0.01
COS φ
LINEAR TRANSMITTED AND RECEIVED

Fig. 6

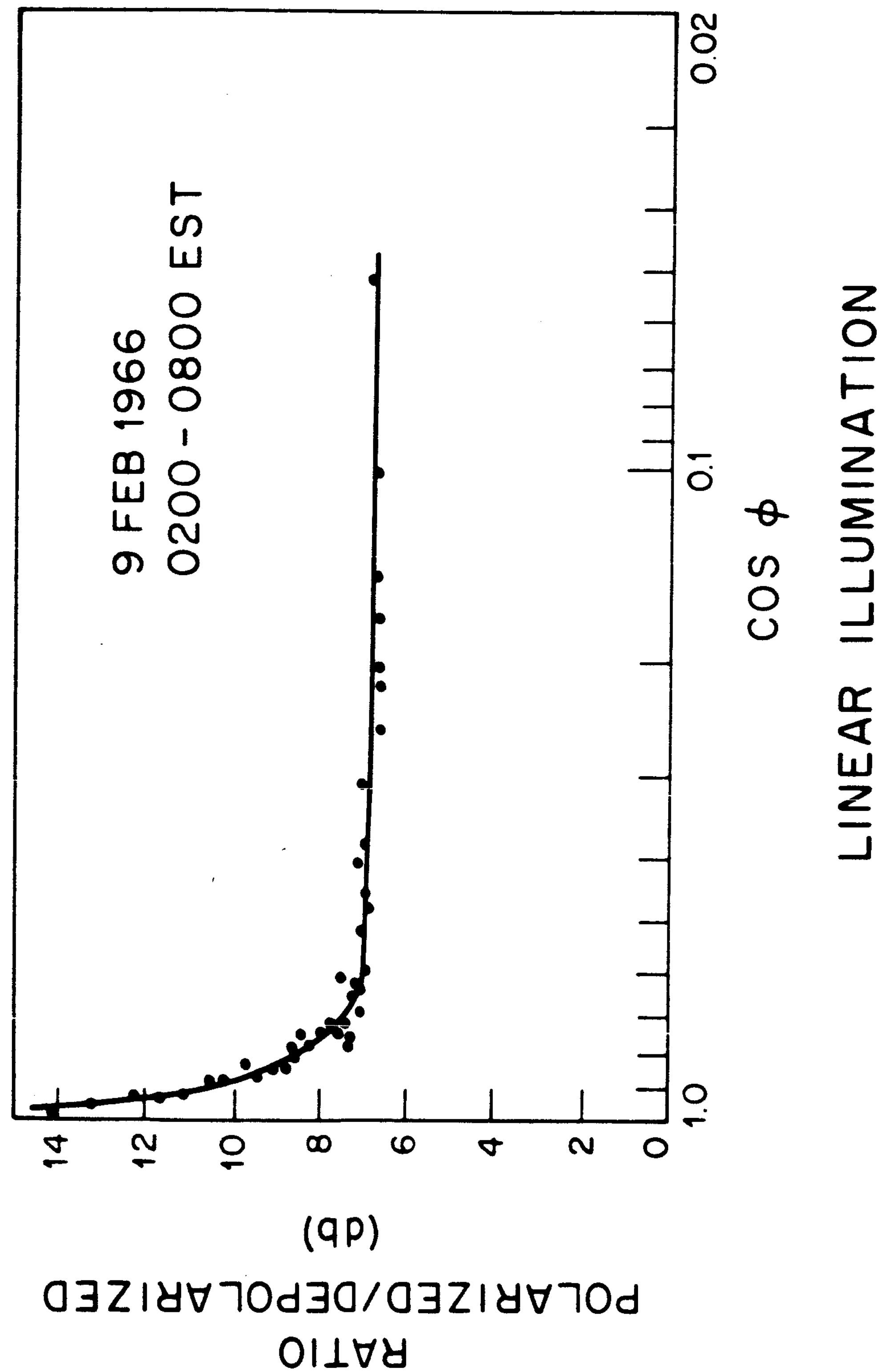
9 FEB 1966
0200 - 0800 EST
COS φ
LINEAR ILLUMINATION
RATIO
POLARIZED/DEPOLARIZED
(db)
0
2
4
6
8
10
12
14
1.0
0.1
0.02

Fig. 7

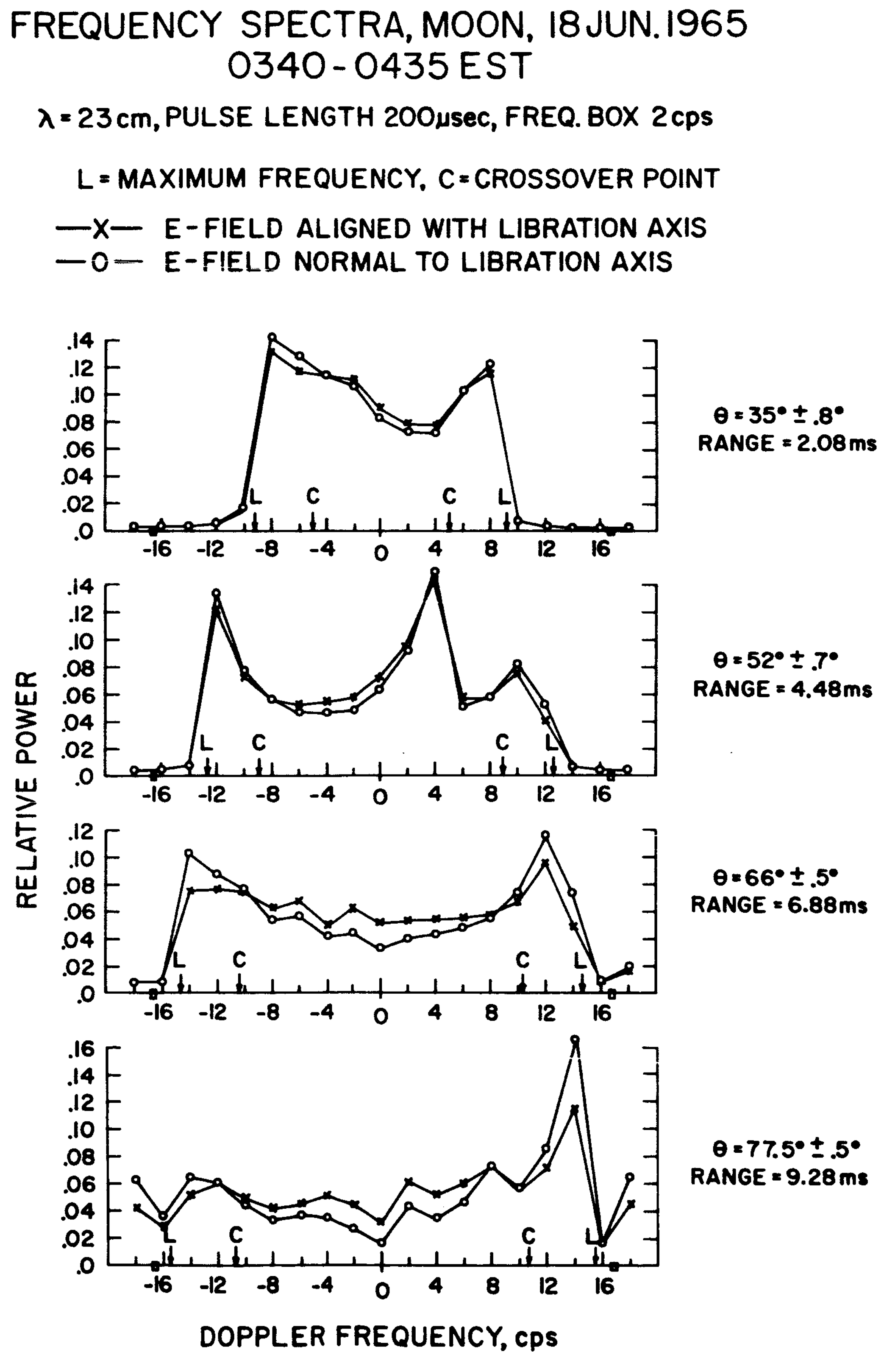
FREQUENCY SPECTRA, MOON, 18 JUN. 1965
0340-0435 EST
λ = 23 cm, PULSE LENGTH 200μsec, FREQ. BOX 2 cps
L = MAXIMUM FREQUENCY, C = CROSSOVER POINT
—X— E-FIELD ALIGNED WITH LIBRATION AXIS
—O— E-FIELD NORMAL TO LIBRATION AXIS
RELATIVE POWER
θ = 35° ± .8°
RANGE = 2.08 ms
θ = 52° ± .7°
RANGE = 4.48 ms
θ = 66° ± .5°
RANGE = 6.88 ms
θ = 77.5° ± .5°
RANGE = 9.28 ms
DOPPLER FREQUENCY, cps

Fig. 8

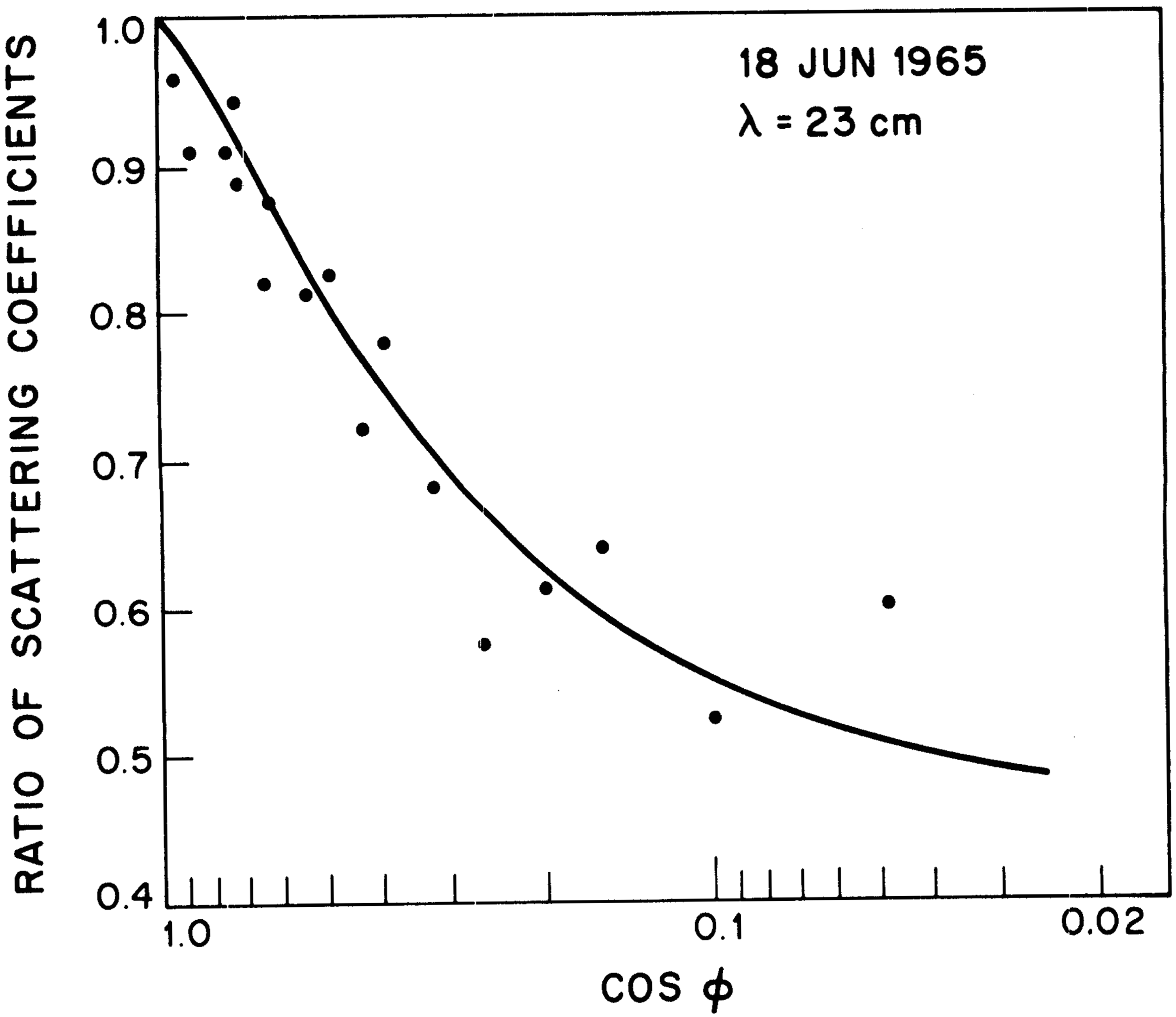

RATIO OF SCATTERING COEFFICIENTS

Fig. 9

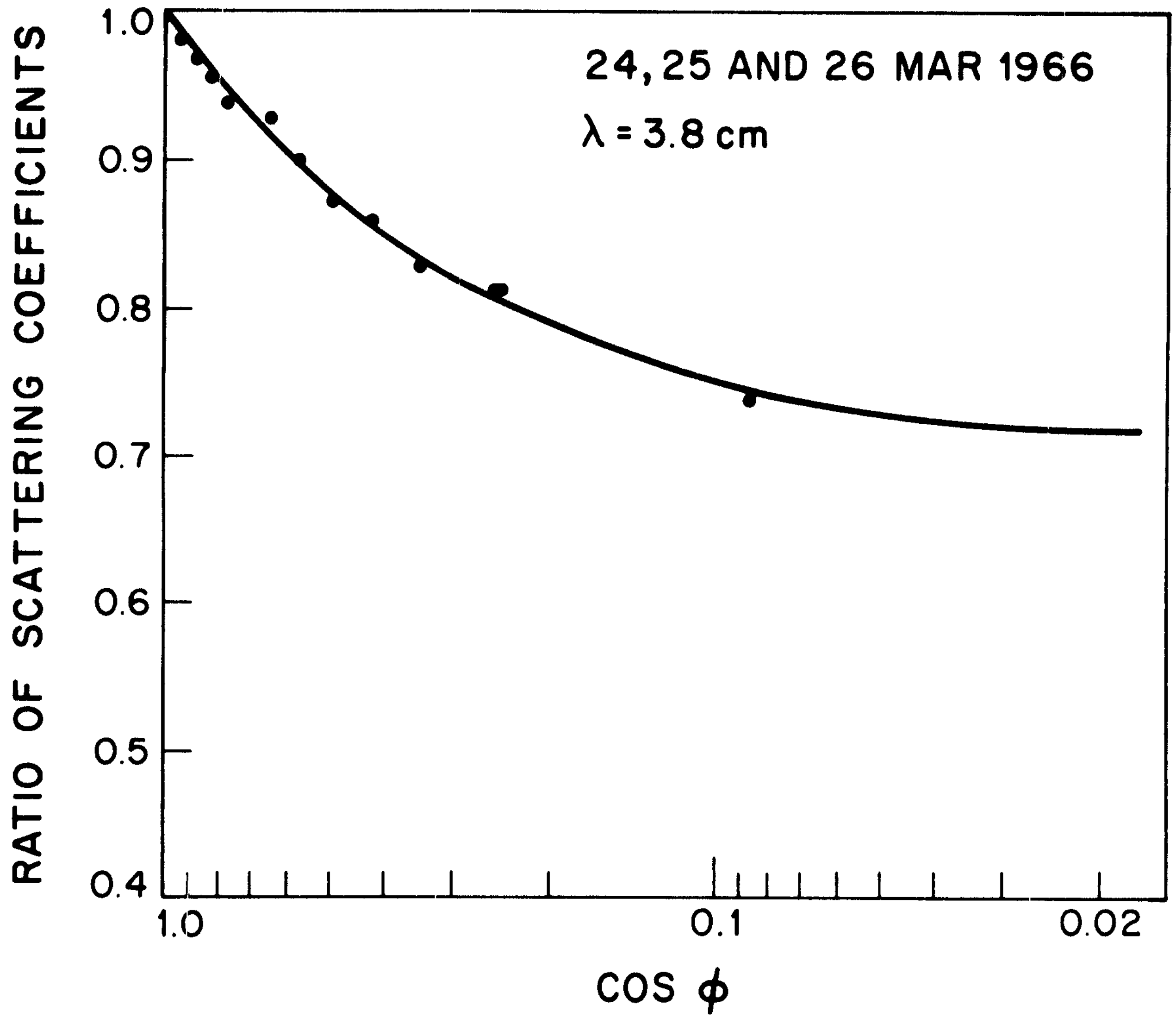

RATIO OF SCATTERING COEFFICIENTS

Fig. 10

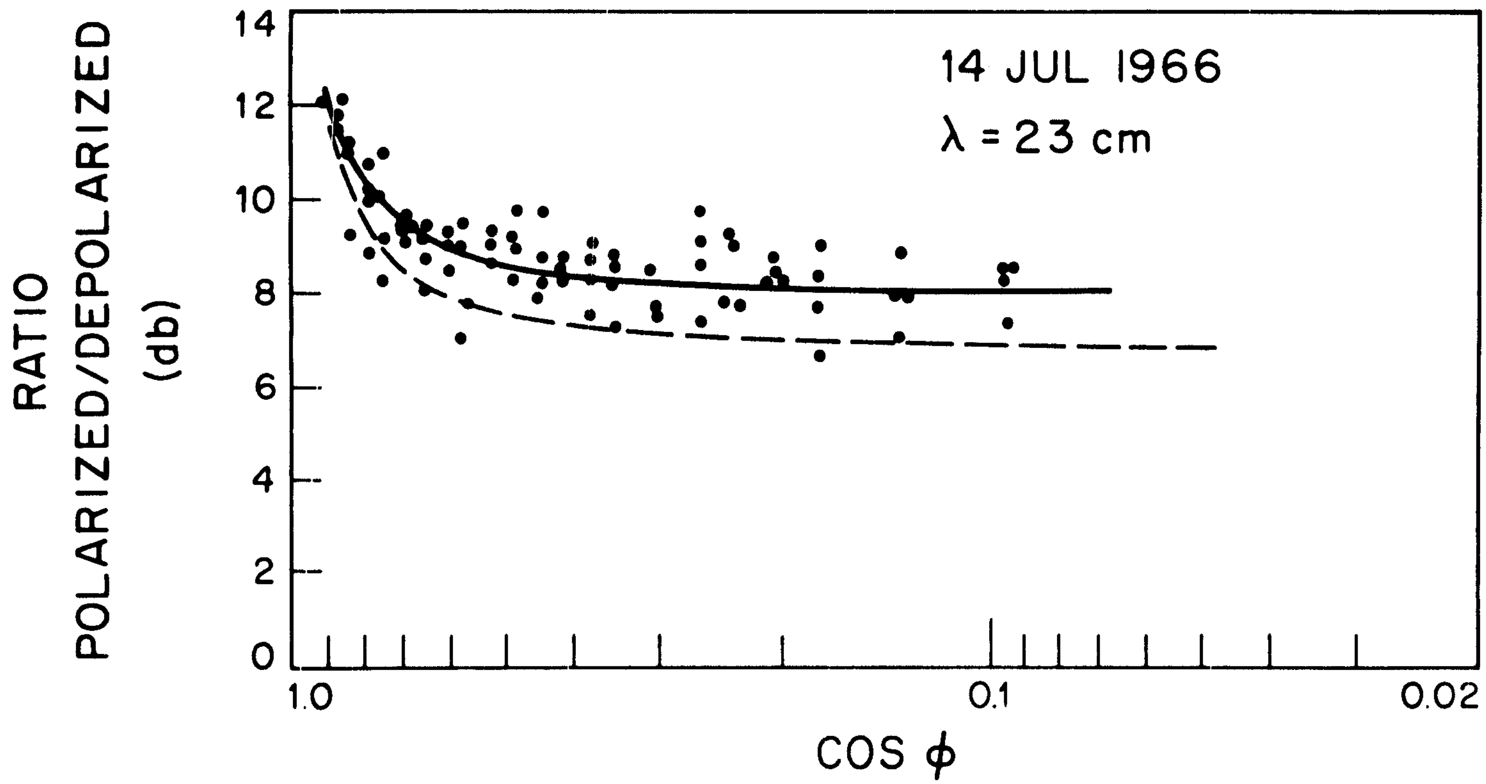

ILLUMINATION LINEAR // PLANE OF INCIDENCE

Fig. 11

POWER REFLECTION COEFFICIENTS FROM DIELECTRIC LAYER OF RANDOM THICKNESS

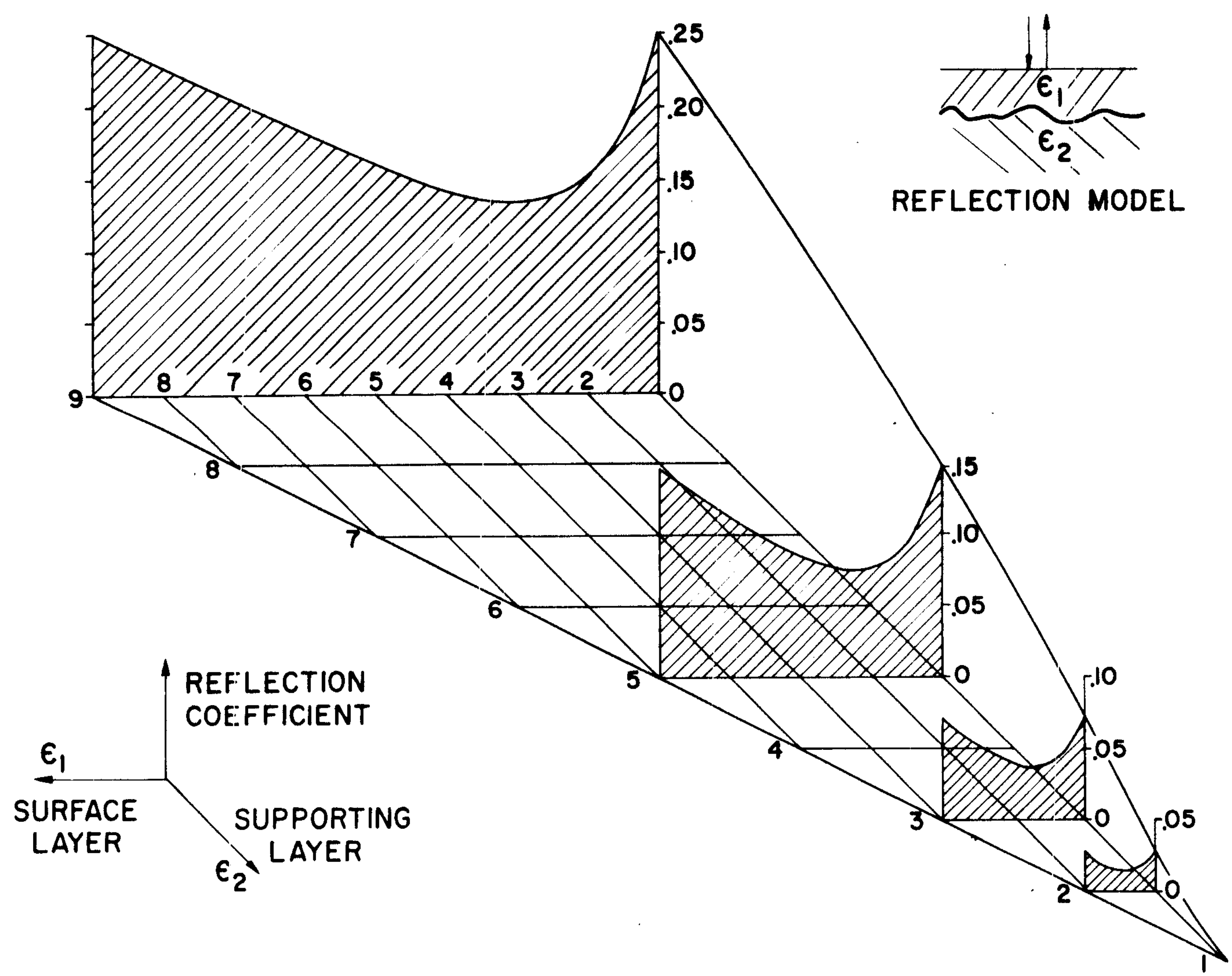

Fig. 12

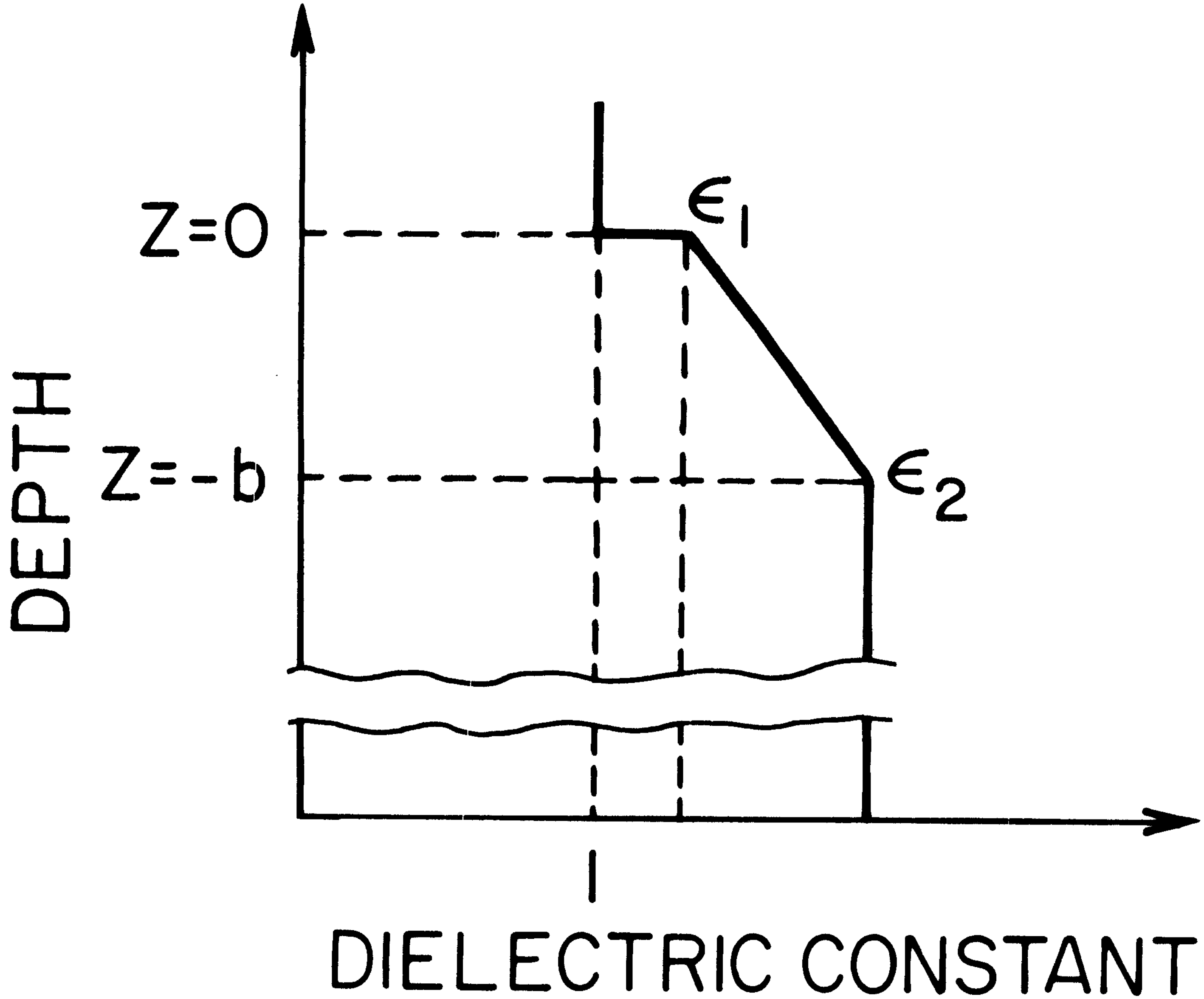

Fig. 13

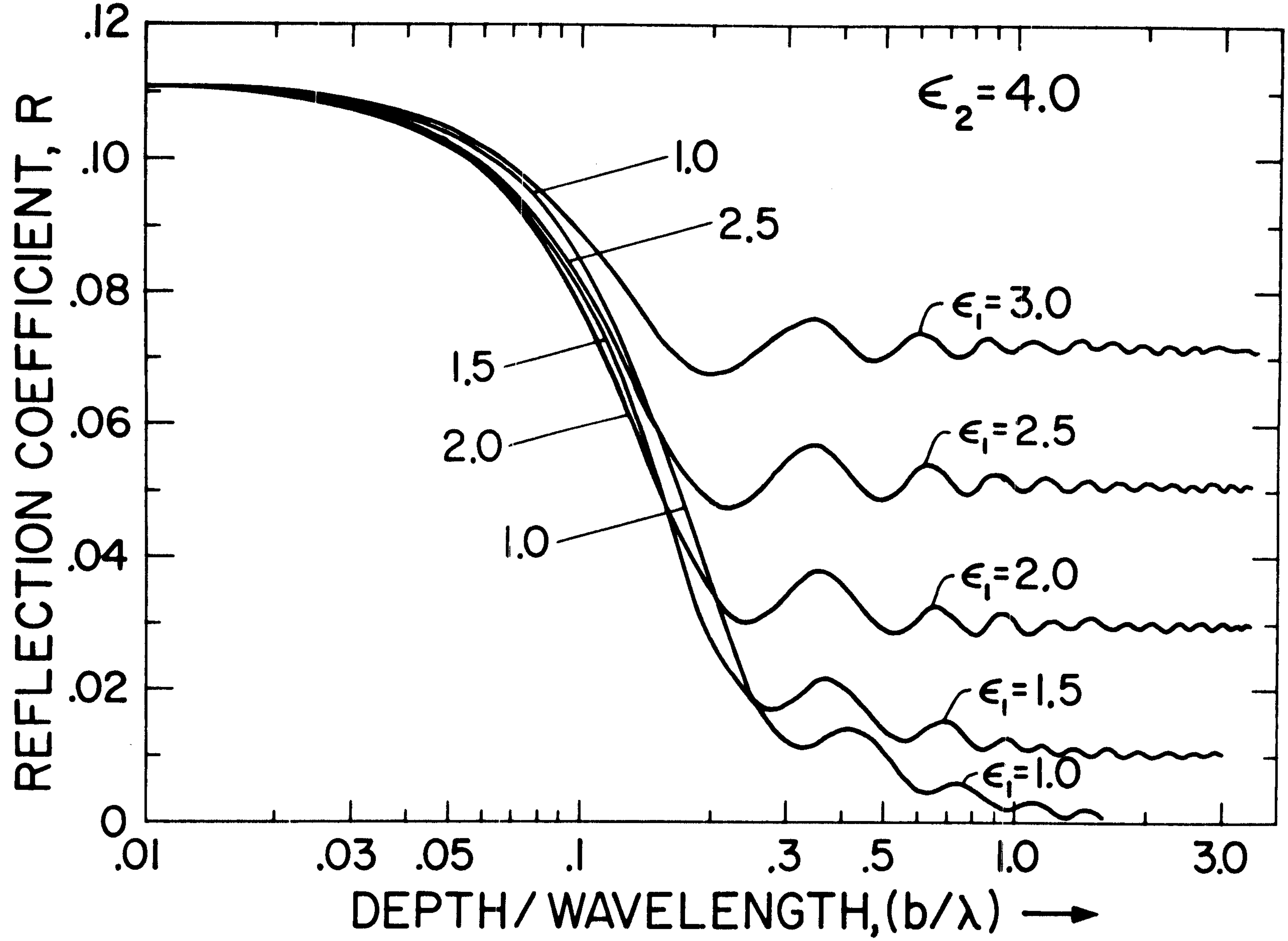

$\epsilon_2 = 4.0$
$\epsilon_1 = 3.0$
$\epsilon_1 = 2.5$
$\epsilon_1 = 2.0$
$\epsilon_1 = 1.5$
$\epsilon_1 = 1.0$
1.0
2.5
1.5
2.0
1.0
.12
.10
.08
.06
.04
.02
0
.01
.03
.05
.1
.3
.5
1.0
3.0
REFLECTION COEFFICIENT, R
DEPTH/ WAVELENGTH, (b/λ) →

Fig. 14

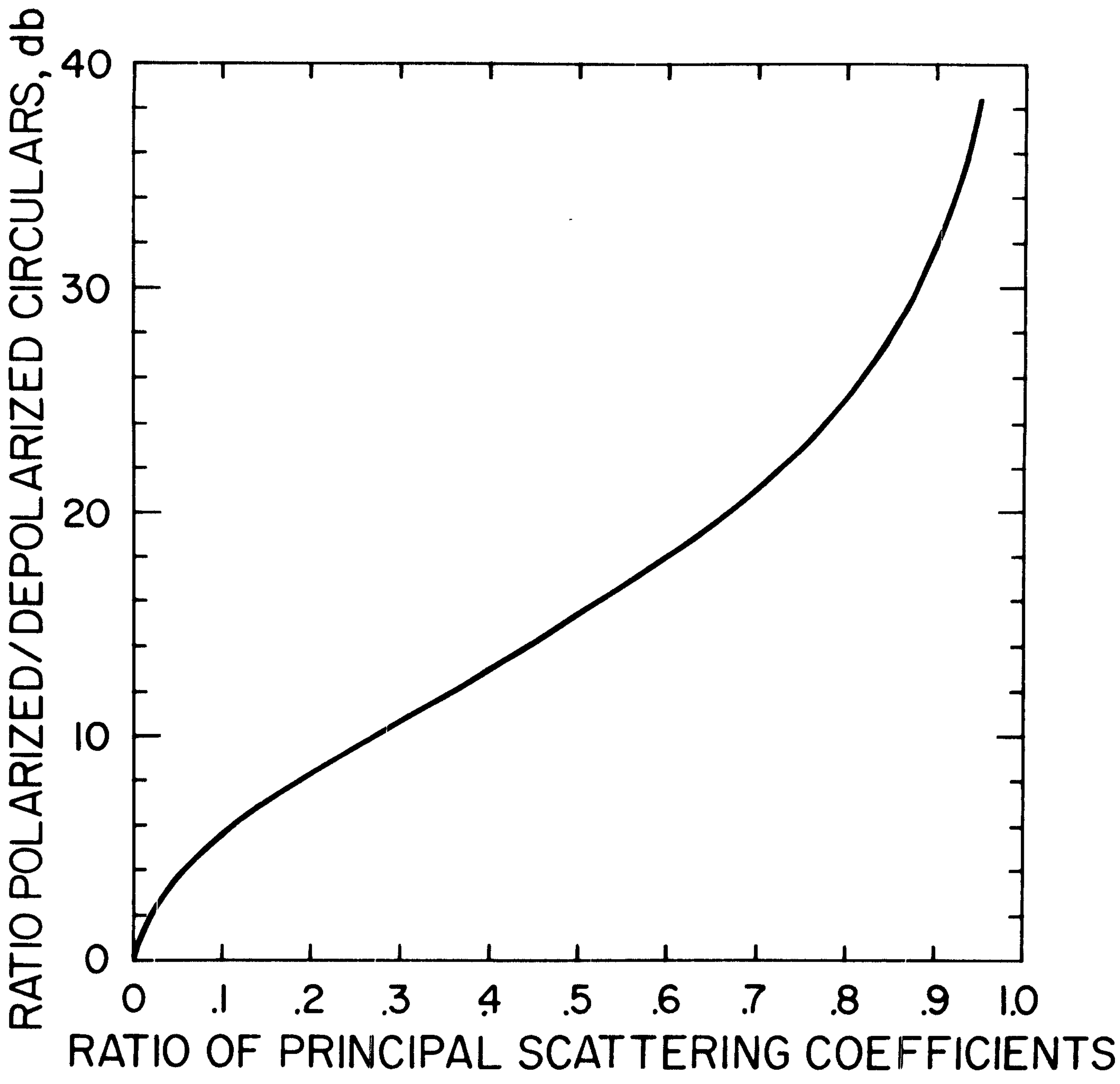
RATIO POLARIZED/DEPOLARIZED CIRCULARS, db
40
30
20
10
0
0
.1
.2
.3
.4
.5
.6
.7
.8
.9
1.0
RATIO OF PRINCIPAL SCATTERING COEFFICIENTS

Fig. 15

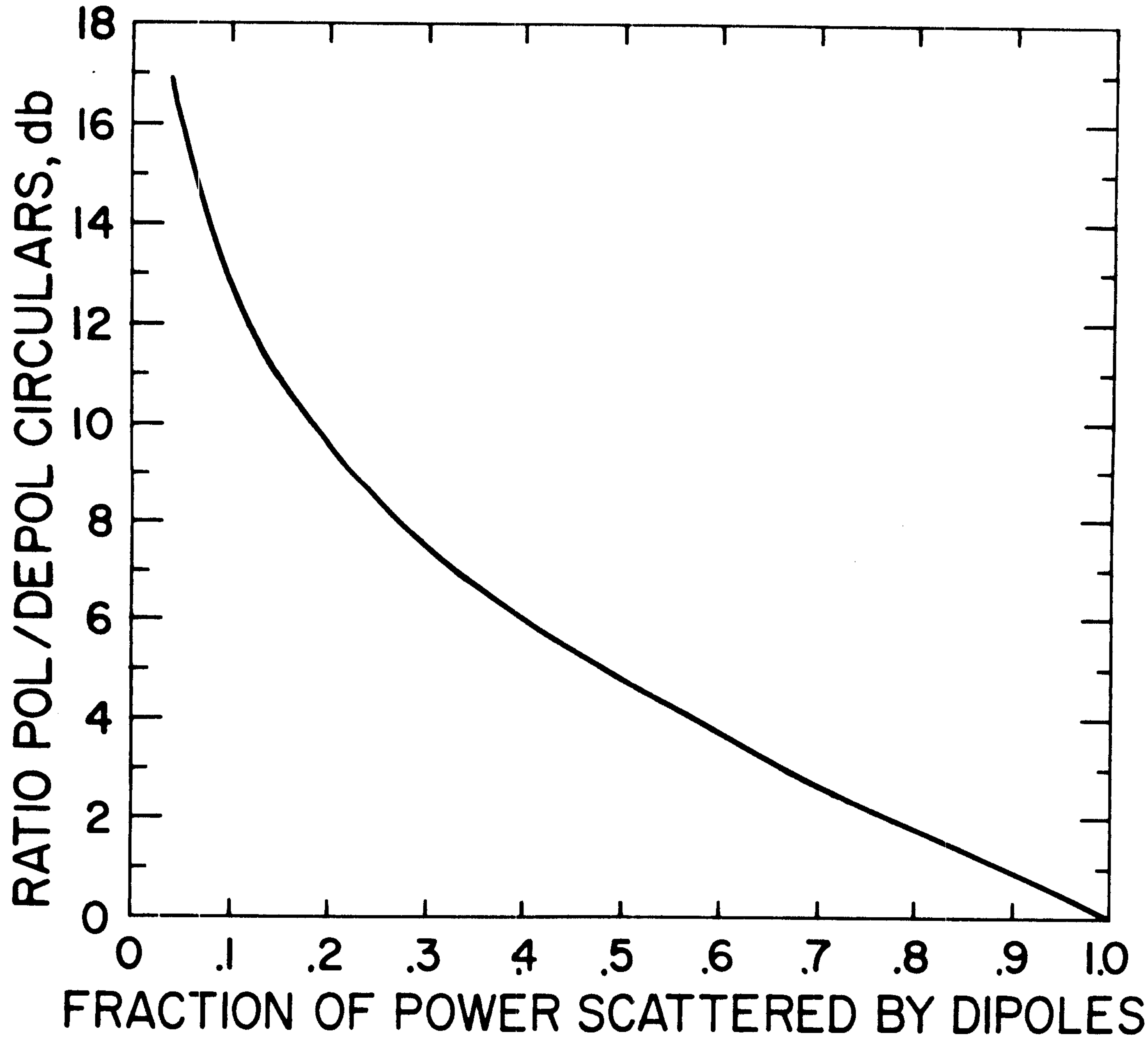
RATIO POL/DEPOL CIRCULARS, db
18
16
14
12
10
8
6
4
2
0
0
.1
.2
.3
.4
.5
.6
.7
.8
.9
1.0
FRACTION OF POWER SCATTERED BY DIPOLES

Fig. 16

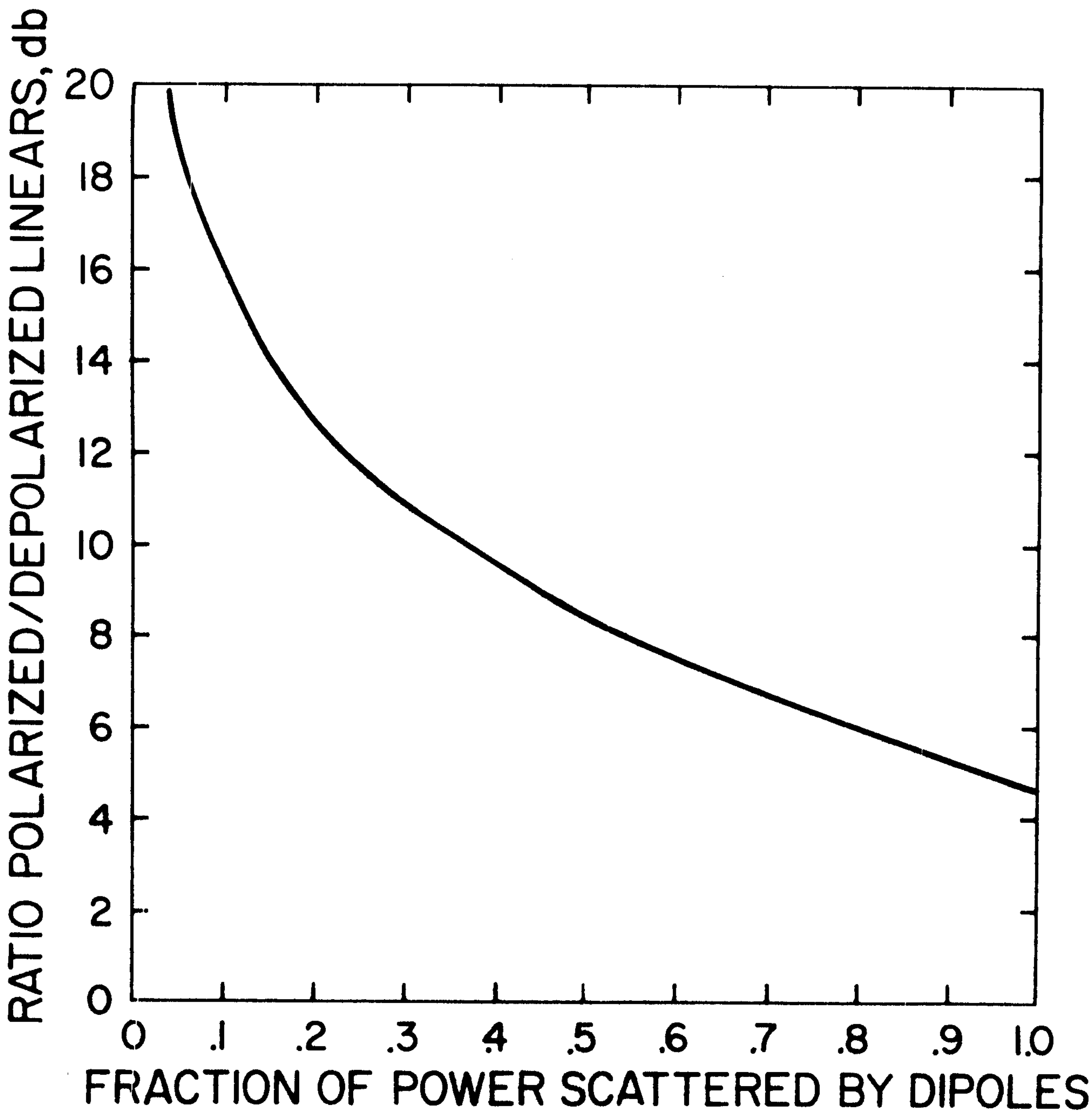
RATIO POLARIZED/DEPOLARIZED LINEARS, db
20
18
16
14
12
10
8
6
4
2
0
0
.1
.2
.3
.4
.5
.6
.7
.8
.9
1.0
FRACTION OF POWER SCATTERED BY DIPOLES

Fig. 17